



1 **A Reanalysis-Based Global Tropical Cyclone Tracks**
2 **Dataset for the Twentieth Century (RGTracks-20C)**

3

4 Guiling Ye^{1,2,3}, Jeremy Cheuk-Hin Leung^{2,4*}, Wenjie Dong^{1,3*}, Jianjun Xu⁵, Weijing Li⁶, Weihong
5 Qian⁷, Hoiio Kong⁴, Banglin Zhang^{2,8}

6 **Affiliations**

7 ¹ School of Atmospheric Sciences, Key Laboratory of Tropical Atmosphere-Ocean System, Ministry of
8 Education, Sun Yat-sen University, Zhuhai, China

9 ² Hunan Institute of Advanced Technology, Changsha, China

10 ³ Southern Marine Science and Engineering Guangdong Laboratory, Zhuhai, China

11 ⁴ Faculty of Data Science, City University of Macau, Macau, China

12 ⁵ CMA-GDOU Joint Laboratory for Marine Meteorology, South China Sea Institute of Marine
13 Meteorology, Guangdong Ocean University, Zhanjiang, China

14 ⁶ National Climate Center, China Meteorological Administration, Beijing, China

15 ⁷ Department of Atmospheric and Oceanic Sciences, Peking University, Beijing, China

16 ⁸ College of Atmospheric Science, Lanzhou University, Lanzhou, China

17

18

19

20 *Corresponding author(s):* Jeremy Cheuk-Hin Leung (chleung@pku.edu.cn); Wenjie Dong
21 (dongwj3@mail.sysu.edu.cn)



22 **Abstract**

23 Tropical cyclones (TCs) are among the deadliest disasters affecting human society, and their
24 response to climate change has widely drawn attention from the public. However, assessing how
25 historical TC activity changed with climate change has proven challenging due to incomplete TC
26 records in the early years. Here, we introduce the Reanalysis-Based Global Tropical Cyclone Tracks
27 Dataset for the Twentieth Century (RGTracks-20C) (Ye et al., 2024), a publicly available century-
28 long global TC track dataset spanning from 1850–2014. The RGTracks-20C is reconstructed from
29 the National Oceanic and Atmospheric Administration Twentieth Century Reanalysis using two
30 independent TC tracking algorithms. Validation based on observations confirms that the RGTracks-
31 20C effectively captures the climatology and long-term variability of TC numbers, tracks, duration,
32 and intensity across various ocean basins. A remarkable key strength of the RGTracks-20C is its
33 ability to fill the missing intensity and location records of TCs observed in early years. This dataset
34 serves as a valuable historical data reference for future research on climate change and TC-related
35 disasters.



36 **1. Introduction**

37 Tropical cyclones (TCs), also known as hurricanes or typhoons, are intense weather systems that
38 form over tropical and subtropical oceans and can cause severe disasters over the coastal regions and
39 even inland areas (Qin et al., 2024; Zhu and Qiring, 2022). Globally, approximately 80 TCs are
40 generated each year (Emanuel, 2018). As one of the most destructive weather systems (Bloemendaal et
41 al., 2022; Dinan, 2017; Emanuel, 2017), TCs significantly impact society and the economy (Kunze, 2021;
42 Lenzen et al., 2019; Noy, 2016). These impacts are expected to be exacerbated by climate change in the
43 future (Chan, 2023; Hassanzadeh et al., 2020; Knutson et al., 2020; Moon et al., 2023; Murakami and
44 Wang, 2022; Yamaguchi et al., 2020). Therefore, research on TCs has become increasingly vital in
45 climate change and prediction (Bhatia et al., 2019; Chan, 2019; Lanzante, 2019; Moon et al., 2019;
46 Sharmila and Walsh, 2018; Zhang et al., 2019). However, past variability of TC activity and underlying
47 mechanisms remains challenging due to incomplete early historical TC observation records, which may
48 lead to controversies (Chan et al., 2022a, b; Knutson et al., 2019; Lee et al., 2020).

49 Previous research has revealed significant issues related to the completeness of historical TC
50 observational data (Lee et al., 2020), which are highly dependent on the development of the global TC
51 observation system, data analysis techniques, and other factors (Klotzbach and Landsea, 2015; Knapp et
52 al., 2010; Kossin et al., 2020; Landsea et al., 2010; Mann et al., 2007; Ying et al., 2014). Before the
53 introduction of satellite observation, TC information (e.g., intensity and location) primarily relied on
54 conventional coastal weather stations and ship observation reports (Landsea et al., 2006, 2008). Aircraft
55 reconnaissance emerged in the North Atlantic (NATL) and western North Pacific (WNP) after World
56 War II (Emanuel, 2008). However, these observational techniques could not capture all occurred TCs
57 due to their limited observation range. It is possible that an existing TC was unrecorded in the early years.
58 In addition, even if a TC was observed and recorded, its track and intensity information may be
59 discontinuous due to the absence of meteorological satellite observations. For instance, there were no
60 observational records of TC wind speeds in the southern hemisphere before 1956 (Emanuel, 2021). Storm
61 intensity in the Indian Ocean is weaker compared to other basins, partly due to the lack of direct coverage
62 by geostationary satellites in that region before 1998 (Schreck et al., 2014). The incomplete observed
63 data of TCs in the early years, mainly before the 1970s, is a commonly-known unsolved issue in the
64 community.

65 Given the limitations of historical TC records, a promising approach is to utilize reanalysis for TC
66 identification (Li et al., 2024; Trachelut and Hart, 2011). Reanalysis combines historical observational
67 data with modern numerical weather models to produce comprehensive, continuous datasets of global
68 atmospheric conditions that adhere to physical principles (Compo et al., 2011; Kalnay et al., 1996; Parker,
69 2016; Slivinski, 2018). The Twentieth Century Reanalysis (20CR) (Compo et al., 2011), provided by the
70 National Oceanic and Atmospheric Administration (NOAA), is a global reanalysis dataset that covers the
71 longest period among all other reanalyses. The 20CR was designed for long-term analyses from
72 individual extreme weather events to climate variability, and has been applied to a wide range of studies,
73 including those on wave height, storm surge, Madden-Julian Oscillations, and TCs (Chand et al., 2022;
74 Cid et al., 2017; Gergis et al., 2020; Lee et al., 2023; Leung et al., 2022; Moore and Babij, 2017; Slivinski
75 et al., 2019; Trachelut et al., 2013; Wang et al., 2012). The fact that the 20CR only assimilates surface



76 pressure and sea level pressure fields, instead of other observations such as satellites and aircraft, makes
77 it less sensitive to the temporal inhomogeneity of observations (Slivinski et al., 2019, 2021).

78 Several independent studies have documented the feasibility of reproducing the characteristics of
79 some historical TC events based on the 20CR (Emanuel, 2010; Lee et al., 2023; Slivinski et al., 2019;
80 Truchelut et al., 2013; Truchelut and Hart, 2011). For example, following Emanuel (Emanuel, 2010),
81 who first expanded and revised TC climatology based on the 20CR, Truchelut and Hart (2011) employed
82 the 20CR to identify previously unknown TCs in the Atlantic and demonstrated that the 20CR can
83 accurately describe large-scale TC thermodynamic structure. Recently, Truchelut et al. (2013) noted that
84 the 20CR has the ability to investigate TC events that were previously undetected in the pre-satellite era.
85 Compared to other reanalyses, the 20CR well captures the intensity of the 1915 Galveston hurricane
86 (Slivinski et al., 2019) and also offers a more accurate representation of landfalling TCs in East Asia (Lee
87 et al., 2023). These previous studies have demonstrated the effectiveness of the 20CR as a tool for
88 characterizing historical TCs (Emanuel, 2010; Truchelut et al., 2013; Truchelut and Hart, 2011). Taking
89 advantage of the 20CR, some researchers have extracted the century-long TC information from the
90 reanalysis product (Chand et al., 2022; Lee et al., 2023; Yeasmin et al., 2023), suggesting its potential as
91 a tool for studying historical changes in TCs under anthropogenic climate change.

92 While the 20CR has been applied to studying the relationship between historical climate change and
93 TC variability, the primary focus was mostly on the TC occurrence frequency, and little attention was
94 given to other TC metrics such as intensity, duration, and location. More importantly, to date, there is no
95 publicly available reanalysis-based global TC dataset covering a century-long period. Therefore, the main
96 objective of this study is to extract TC information (including location, intensity, and lifetime) from the
97 20CR and reconstruct a historical global TC track dataset spanning 1850–2014. The produced dataset is
98 named the Reanalysis-Based Global Tropical Cyclone Tracks Dataset for the Twentieth Century
99 (RGTracks-20C) and is open to the public for research use. This paper first introduces the production
100 details of the RGTracks-20C and then discusses the validity, key strengths, and usage notes of the datasets.
101 We anticipate that the RGTracks-20C will provide valuable insights into the changing patterns of
102 historical TC activity, improving our understanding of the response of TCs to climate change.

103 **2. Data and methods**

104 **2.1 Data**

105 The primary objective of this study was to reconstruct a 20th century global TC dataset from the
106 20th Century Reanalysis version 3 (20CRv3) (Slivinski et al., 2019, 2021), the latest version of the 20CR
107 produced by NOAA. Then, the validity of the reconstructed 20th century global TC data was evaluated
108 based on the observed TC records, i.e., the International Best Track Archive for Climate Stewardship
109 (IBTrACS) dataset (Knapp et al., 2010).

110 **2.1.1 20th Century Reanalysis**

111 The 20CRv3 is led by NOAA's Physical Sciences Laboratory (PSL) and the Cooperative Institute
112 for Research in Environmental Sciences (CIRES) at the University of Colorado, supported by the U.S.
113 Department of Energy (DOE) (Slivinski et al., 2019, 2021). It, by combining advanced data assimilation



114 and numerical prediction techniques with historical observation data, provides long-term historical
115 weather data with diverse variables, complete spatial and temporal coverage. The 20CRv3 employs sea-
116 surface temperature and sea-ice distributions as its boundary conditions and assimilates only surface
117 pressure reports from the International Surface Pressure Databank (ISPD) version 4.7 (Compo et al., 2019;
118 Cram et al., 2015), which include observations from stations and ships, as well as TC intensity (the
119 minimum central pressure (SLP_{min}) from the IBTrACS (Knapp et al., 2010). As such, it is more consistent
120 and homogeneous with time than other reanalyses (Slivinski et al., 2019).

121 One should note that the IBTrACS and 20CRv3 are not two independent datasets because the SLP_{min}
122 records in the IBTrACS are partly assimilated in the production of 20CRv3. However, reports show that
123 20CRv3 shows TCs structure and intensity more accurately and closer to observations than other 20th
124 century reanalyses as a result of the assimilation of IBTrACS (Laloyaux et al., 2018; Slivinski et al.,
125 2019). And, it provides a four-dimensional global gridded atmospheric dataset that spans the whole 20th
126 century and part of the 19th century (1836–2015, with an experimental extension spanning 1806–35),
127 with a 3-hour temporal resolution and $1^\circ \times 1^\circ$ horizontal resolution (Slivinski et al., 2021). Thus, the
128 20CRv3 was applied to the production of the RGTracks-20C in this paper.

129 2.1.2 IBTrACS

130 The IBTrACS (Knapp et al., 2010), published by the NOAA, merges recent and historical TC data
131 from meteorological agencies worldwide. These include the Regional Specialized Meteorological
132 Centers (RSMC) and Tropical Cyclone Warning Centers (TCWC) of the World Meteorological
133 Organization (WMO), as well as non-WMO Centers, such as the China Meteorological Administration,
134 the Hong Kong Observatory and the Joint Typhoon Warning Center. The IBTrACS is the most
135 comprehensive and publicly available global TC best-track dataset. It has been widely applied in previous
136 research to investigate the characteristics of TCs (Lai et al., 2020; Li et al., 2023; Tu et al., 2021, 2022;
137 Wang and Toumi, 2022; Zhang, 2023), and has served as a criterion for assessing TC records derived
138 from reanalysis (Bell et al., 2018; Bourdin et al., 2022; Chand et al., 2022; Hodges et al., 2017; Lee et al.,
139 2023). In this study, the most updated version of IBTrACS (v04) (Knapp et al., 2018) serves as an
140 observation reference for evaluating the reliability of the RGTracks-20C. This dataset was cleaned before
141 being used for analyses. Details about the data pre-processing procedures are referred to in Figure B1 in
142 Bourdin et al. (2022). In particular, we standardized maximum sustained wind speeds ($WIND_{max}$) in
143 IBTrACS to 10-minute sustained wind speeds to ensure a consistent global standard (Knapp et al., 2010).
144 We then removed tracks that did not reach the tropical storm stage ($WIND_{max} < 16 \text{ m} \cdot \text{s}^{-1}$) and those that
145 lasted shorter than two days.

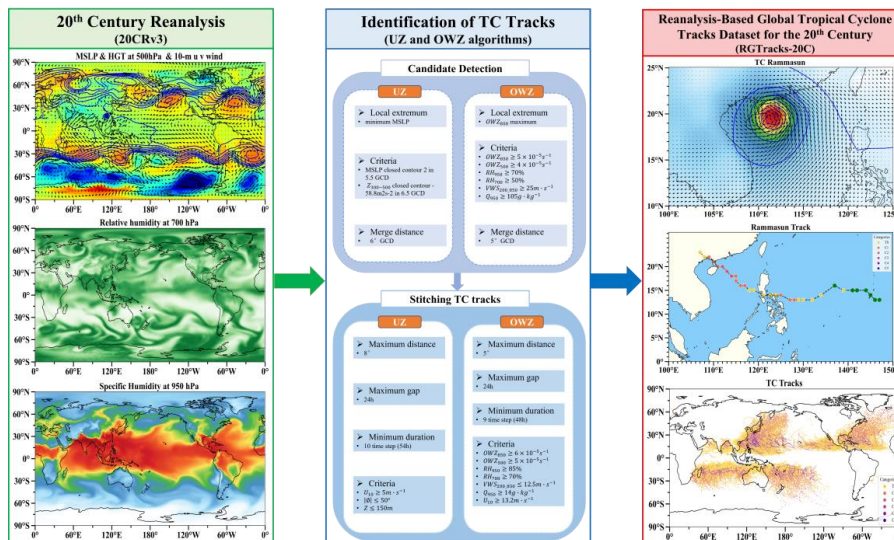
146 Although the IBTrACS has time coverage dating back to the early 20th century, we utilize the data
147 only for the post-satellite period (1979–2014) due to the early data incompleteness issues (Chang and
148 Guo, 2007; Lee et al., 2020; Truchelut et al., 2013). Given that the IBTrACS is the most reliable record
149 of TCs after the 1970s, the IBTrACS serves as the best benchmark for validating the data quality of
150 RGTracks-20C. However, because the starting years of records vary across basins within the IBTrACS,
151 biases may occur in the assessment results (see Supplementary Sects. S2.2 and S2.4 for more details).



152 **2.2 Production of the RGTracks-20C**

153 **2.2.1 Procedure**

154 The RGTracks-20C was constructed from the latest version of 20CR (20CRv3). The relatively short
 155 and imperfectly sampled observational record of TCs introduces considerable uncertainty in their data
 156 over the past century (Landsea, 2007; Landsea et al., 2010), hindering accurate detection of interannual
 157 variability and long-term trends (Knutson et al., 2019; Lee et al., 2020). Reanalysis is an effective way
 158 to reduce this uncertainty (Chand et al., 2022; Truchelut et al., 2013). Since TC information is not directly
 159 provided in the 20CRv3, objective TC trackers were applied to detect and track TCs in this dataset.
 160 Numerous trackers have been developed by operational centers and research institutions to meet various
 161 application needs (Hodges et al., 2017; Horn et al., 2014; Tory et al., 2013; Zarzycki and Ullrich, 2017).
 162 In this study, as the first version of the RGTracks-20C, we applied two widely used, publicly available,
 163 and effective trackers: (1) the physically-based Ullrich & Zarzycki (UZ) tracker (Zarzycki and Ullrich,
 164 2017) and (2) the dynamics-based Okubo-Weiss-Zeta (OWZ) tracker (Tory et al., 2013). Both trackers
 165 have been reported to effectively capture TC systems from coarse resolution gridded data uncertainty
 166 (Chand et al., 2022; Truchelut et al., 2013), such as the 20CRv3. Figure 1 shows the procedure of
 167 producing the RGTracks-20C, and details of the methodology are provided in the following.
 168



169 **Figure 1: Schematic diagram showing the production of the RGTracks-20C from the 20CRv3 based on the**
 170 **UZ and OWZ tracking algorithms. Variables shown include U10: 10-m wind speed, ϕ : latitude, z:altitude,**
 171 **GCD: great circle distance.**
 172

173 **2.2.2 TC tracker**

174 **i. OWZ Tracker**

175 The OWZ tracker, initially proposed by Tory et al. (2013), is designed to detect low-deformation
 176 vorticity regions within large-scale disturbances, typically situated within the so-called "marsupial



177 pouch", which have the potential for tropical storm formation. Given that the OWZ approach relies solely
 178 on large-scale variables, it is particularly effective in detecting TC in coarse-resolution models or
 179 reanalysis (Bell et al., 2018; Bourdin et al., 2022).

180 The OWZ tracker involves a low-deformation vorticity variable parameter, which is the product of
 181 absolute vorticity and the Okubo-Weiss parameter normalized by the vertical components of relative
 182 vorticity squared (Eq. 1):

$$183 \quad OWZ = \text{sgn}(f) \times (\zeta + f) \times \max \left[\frac{\zeta^2 - (E^2 + F^2)}{\zeta^2}, 0 \right] \quad (1)$$

184 where f is the Coriolis parameter, $\zeta = \partial v / \partial x - \partial u / \partial y$ is the vertical component of relative vorticity,
 185 $(\zeta + f)$ is the absolute vorticity, E is the stretching deformation (Eq. 2), and F is the shearing
 186 deformation (Eq. 3):

$$187 \quad E = \frac{\partial u}{\partial x} - \frac{\partial v}{\partial y} \quad (2)$$

$$188 \quad F = \frac{\partial v}{\partial x} + \frac{\partial u}{\partial y} \quad (3)$$

189 **First step: Candidate detection.**

190 The OWZ tracker begins by identifying local maxima of OWZ at 850 *hPa*. Any candidate with a
 191 stronger OWZ maximum within 5° of great circle distance (GCD) is excluded. Next, only candidates that
 192 meet the six initial threshold conditions shown in Table 1 within a 2° GCD of the identified maximum
 193 are retained. Based on the information provided in Table 1, besides the required minimum threshold
 194 values for the OWZ parameter at 850 *hPa* and 500 *hPa*, additional dynamical and thermodynamic
 195 parameters related to TC formation are taken into account. These parameters include the maximum
 196 threshold for the wind vector difference (vertical wind shear) between 850 *hPa* and 200 *hPa*, as well as
 197 the relative humidity at 950 *hPa* and 700 *hPa*, and the minimum threshold for the specific humidity at
 198 950 *hPa*. This step primarily aims to identify grid points that contain essential components of a storm.
 199 Subsequently, neighboring grid points are grouped together to define potential TCs.

200 **Second step: Stitching TC tracks.**

201 Consecutive TC points are linked together if their distance does not exceed 5° of GCD and there is
 202 a maximum gap of 24 hours between them. To be considered as a valid TC, additional core thresholds
 203 (shown in Table 1) must be met for at least 9 time-steps (48 hours). Finally, tracks that do not maintain
 204 tropical storm intensity (wind speed at 10 m $\geq 12.3 \text{ m} \cdot \text{s}^{-1}$) for at least 1 time step are excluded.

205

206 **Table 1. Parameter threshold values for the OWZ detection criteria. Subscripts stand for isobaric**
 207 **levels in *hPa* (OWZ: Obuko-Weiss-Zeta s^{-1} , RH: relative humidity %; VWS: vertical wind**
 208 **shear $\text{m} \cdot \text{s}^{-1}$; Q: specific humidity $\text{g} \cdot \text{kg}^{-1}$.)**

Criterion	OWZ ₈₅₀	OWZ ₅₀₀	RH ₉₅₀	RH ₇₀₀	VWS _{200_850}	Q ₉₅₀
Initial	50×10^{-6}	40×10^{-6}	70	50	25	10
Core	60×10^{-6}	50×10^{-6}	85	70	12.5	14

209

210



211 **ii. UZ tracker**

212 The UZ tracker, originally proposed by Zarzycki and Ullrich (2017), utilizes sea level pressure on
213 the model grid, incorporating criteria for warm-core structures and storm lifetime.

214 **First step: Candidate detection.**

215 Initially, candidates are identified based on the SLP minimum. And, only those candidates that meet
216 the following two closed-contour criteria are kept:

217 1. An increase in SLP minimum of at least 2 hPa within a 5.5° GCD from the candidate point to
218 ensure the presence of a sufficiently strong and coherent low-pressure area.

219 2. The geopotential thickness between 300 and 500 hPa (denoted as $Z_{300-500}$) must decrease by
220 $58.8 \text{ m}^2 \text{ s}^{-2}$ over a distance of 6.5° GCD from the maximum center of $Z_{300-500}$ within 1° GCD of the
221 center of minimum SLP.

222 Finally, candidates with a stronger SLP minimum within a 6°=GCD are excluded.

223 **Second step: Stitching TC tracks.**

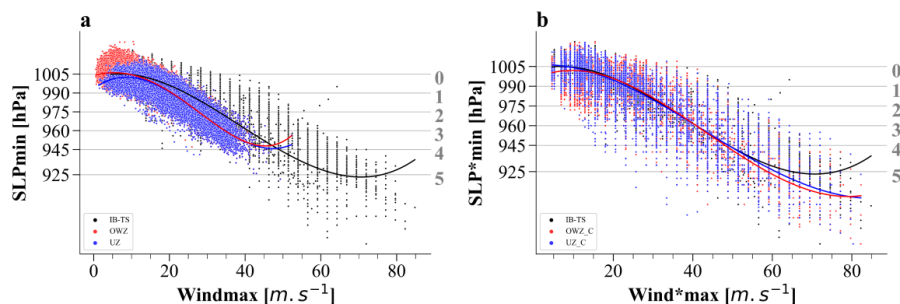
224 The candidates are subsequently linked in time to create paths, ensuring a maximum distance of 8°
225 GCD between candidates. Each path must last for at least 54 hours without gaps longer than 24 hours.
226 Additionally, ten 6-hourly time steps (equivalent to 54 hours) must satisfy the following thresholds: wind
227 speed at 10m $\geq 10 \text{ m/s}$ and $z \leq 150 \text{ m}$ (where z represents the altitude), and the storm must form
228 between 0° and 50°.

229 The UZ tracker, developed specifically for high-resolution models and reanalysis data, is designed
230 to maintain a low false-alarm rate, which may lead to a larger number of misses of weaker storms (Roberts
231 et al., n.d.). In contrast, the OWZ tracker, based on the large-scale environmental conditions favorable
232 for TC formation, addresses this limitation. Thus, combining these two TC trackers can effectively
233 enhance the reliability of RGTracks-20C.

234 A command-line software, TempestExtremes, developed by Zarzycki and Ullrich (2017), enables
235 fast and versatile and versatile implementation of TC trackers, was used in this study. For further details,
236 please refer to Ullrich et al. (2021).

237 **2.2.3 Bias Correction of TC intensity**

238 Given the low horizontal resolution in the 20CRv3, TC intensities derived directly from the
239 reanalysis generally underestimated compared to observations (Fig. 2a) (Bourdin et al., 2022; Roberts et
240 al., n.d.). To address this issue, a quantile mapping bias correction, similar to the method used by Zhao
241 and Held (2010), was applied to adjust for the TC intensity bias within the dataset. The main idea is to
242 fit the 20CRv-derived TC intensity distributions, either probability distribution functions (PDFs) or
243 cumulative distribution functions (CDFs), to the observed distributions. This method has demonstrated
244 significant efficacy in enhancing the accuracy of TC intensity within models or reanalyses (Faranda et
245 al., 2023; Yoshida et al., 2017). This adjustment resulted in a wind-pressure relationship in RGTracks-
246 20C that aligns more closely with observational data (Fig. 2b).



247
 248 **Figure 2: Wind–pressure relationships for IBTrACS and RGTracks-20C. a–b, Scatter plots of SLPmin (unit:**
 249 **hPa) against maximum sustained wind speeds (WINDmax) (unit: $m \cdot s^{-1}$), based on the TCs from IBTrACS**
 250 **(black), OWZ (red), and UZ (blue) trackers, before (a) and after (b) intensity bias correction (see Methods).**
 251 **The curves represent fourth-order polynomial fit results. Storm categories, as defined in the section 'TC**
 252 **intensity', are indicated by horizontal gray lines.**

253

254 2.3 Verification of RGTracks-20C

255 2.3.1 Tracks matching

256 After utilizing the UZ and OWZ trackers to detect TC vortices from the 20CRv3, the resulting tracks
 257 are matched one-to-one with those observed in the International Best Track Archive for Climate
 258 Stewardship (IBTrACS). The specific procedures are detailed in the "2.4 Tracks Matching" section by
 259 Bourdin et al. (2022).

260 Specifically, a detected track D consists of n points (d_1, d_2, \dots, d_n) corresponding to the moments ($t_1,$
 261 t_2, \dots, t_n). Similarly, a track O observed in IBTrACS consists of a collection of points at a given time. For
 262 every point $d_i (t_i)$ on track D, points from O at the same time t_i located within a 300 km radius of d_i are
 263 linked. There may be instances where no such points are found in O. The subset of points in O that are
 264 linked to any point in D is labeled as $O_{D-paired}$. It consists of $|O_{D-paired}|$. There are three possible scenarios:

- 265 1. $|O_{D-paired}| = 0$: If none of the points in the RGTracks-20C track D match any points in track O,
 266 then track D is classified as a False Alarm (FA).
- 267 2. $|O_{D-paired}| > 0$: If all points in $O_{D-paired}$ track correspond to points in the same observed track O,
 268 then track O is identified as the closest match for D.
- 269 3. $|O_{D-paired}| > 0$: If the points in $O_{D-paired}$ correspond to several observed tracks in O, the observed
 270 track with the most points paired with D is regarded as the best match for D.

271

272 2.3.2 Track verification

273 Following the approach suggested by Bourdin et al. (2022), this study compares TC tracks detected
 274 from the 20CRv3 with observed tracks from the IBTrACS. The probability of detection (POD) (Eq. 4)
 275 and false alarm rate (FAR) (Eq. 5) are used to assess the detection skills of the two trackers.

$$276 \quad POD = \frac{H}{H + M} \quad (4)$$



277

$$278 \quad FAR = \frac{FAs}{H + FAs} \quad (5)$$

279 where hits (H) refer to TC tracks detected from the 20CRv3 that are also present in IBTrACS, misses (M)
 280 denote those tracks that are recorded in IBTrACS but were not detected in the 20CRv3, and false alarms
 281 (FAs) refer to non-existing TCs that were detected from the 20CRv3.

282 2.4 Definitions

283 2.4.1 TC intensity

284 In assessing the TC intensity, SLP_{min} and $WIND_{max}$ are two commonly used metrics in TC research.
 285 However, because $WIND_{max}$ in both observations and reanalysis exhibits relatively higher uncertainties
 286 (Bourdin et al., 2022; Chavas et al., 2017; Knapp et al., 2010; Knutson et al., 2015; Schreck et al., 2014),
 287 this study opted to use SLP_{min} as the only indicator of TC intensity when verifying the validity of
 288 RGTracks-20C. Nevertheless, $WIND_{max}$ of detected TCs is also provided in the RGTracks-20C (Table 2)
 289 as a reference for researchers who wish to use and improve the dataset, though it is not discussed in the
 290 paper.

291

292 **Table 2.** Data format of the RGTracks-20C. track_id: storm identifier, lat: latitude degrees_north,
 293 lon: longitude degrees_east, SLPmin: minimum central pressure (unit: hPa), WINDmax:
 294 maximum wind speed (units: $m \cdot s^{-1}$), WIND*max and SLP*min denotes TC intensities after bias
 295 correction.

track_id	year	month	day	hour	lon	lat	$WIND_{max}$	SLP_{mi}	hemisphere	basin	season	$WIND^*_{max}$	SLP^*_{mi}
0	1979	1	1	0	142.00	15.00	13.57	996.09	S	SP	1979	13.57	990.00
0	1979	1	1	6	144.00	15.00	14.95	995.27	S	SP	1979	14.95	980.27
...
...
...
2880	2014	12	31	18	120.00	9.00	11.122	1006.20	N	WNP	2014	22.12	998.20

296

297 **Storm categories:** the Saffir-Simpson Hurricane Scale (SSHS) from 1 to 5 based on their peak 1-
 298 minute wind speed at 10 meters above the surface. In this study, given the significant uncertainties in
 299 WINDmax due to differences between institutions and the limitations of model simulation capabilities
 300 (Chavas et al., 2017; Klotzbach et al., 2020; Knutson et al., 2015), we have chosen to classify based on
 301 SLPmin, following the definition of Klotzbach et al. (2020).

302 2.4.2 Basins

303 We explore the performance of TCs in RGTracks-20C on global and regional scales. The regional
 304 division is mainly based on the appendix guide of Knutson et al. (2015), which divides the globe into six
 305 basins: the WNP, ENP, South Pacific (SP), NI, South Indian (SI), and NATL.



306 2.4.3 TC days

307 TC days is defined as the number of 6-hour periods during which an active TC occurs within a basin,
308 divided by 4 (to convert 6-hour blocks into days) and accumulated for the year under consideration such
309 that:

$$310 \quad TC \text{ days} = \frac{1}{4} \sum_{i=0}^n L_i \quad (6)$$

311 where L_i is the individual lifetime of a TC within the bounds of a basin.

312 3. Results and discussion

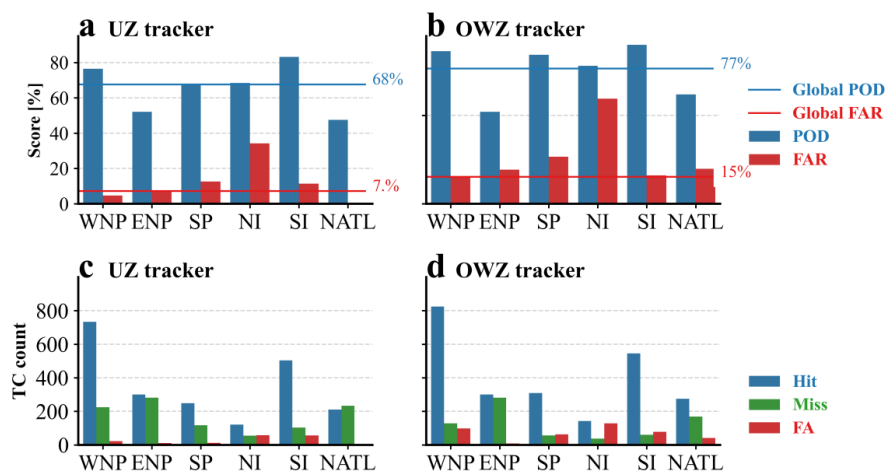
313 3.1 Data Records

314 The constructed RGTracks-20C (Ye et al., 2024) provides a century-long collection of global TCs
315 identified from the 20CRv3. The RGTracks-20C is publicly available at the
316 <https://github.com/jeremychleung/RGTracks-20C/> and <https://zenodo.org/record/8410597>. This dataset
317 provides detailed TC information, including location (longitude, latitude, hemisphere, and basin), time
318 (year, month, day, hour, and season), and intensity (SLP_{min} and $WIND_{max}$), with a temporal resolution of
319 6 hours, spanning from 1850 to 2014 and covering the globe. The dataset is provided as a comma
320 separated values (.csv) file and has a format similar to that of the IBTrACS (Table 2). It is noted that, in
321 the RGTracks-20C, $WIND_{max}$ serves, in addition to SLP_{min} , as a supplementary reference of TC intensity
322 for researchers, but is not discussed here due to accuracy issues and should be used cautiously.

323 3.2. Validity of trackers

324 As documented in prior studies, biases are unavoidable when extracting TCs from reanalyses, given
325 the limitations of reanalysis in reproducing the high-resolution TC structure and circulation patterns, as
326 well as the errors caused by the application of different trackers (Bell et al., 2018; Horn et al., 2014; Lee
327 et al., 2023; Slivinski et al., 2019; Truchelut et al., 2013). Before verifying the reliability of RGTracks-
328 20C, it is necessary to evaluate the performance of the two trackers applied.

329 The POD and FAR of TCs identified by the UZ and OWZ trackers are calculated to assess the ability
330 of the trackers to detect TCs from the 20CRv3 globally and across six basins (see Track verification).
331 Globally, the overall POD and FAR of TCs detected by the UZ tracker are 68% and 7% (Fig. 3a), while
332 those by the OWZ tracker are 77% and 15%, respectively (Fig. 3b). Detailed comparisons of each
333 component of POD and FAR, including the number of hits, false alarms, and misses, are provided in
334 Supplementary Sect. S1 and Fig. S1.



335

336

337

338

339

340

341

Figure 3: Accuracy of TC number detection of the RGTracks-20C. a–b, POD (blue bars and line, unit: %) and FAR (red bars and line, unit: %) for TC number detected by the UZ (a) and OWZ (b) trackers in each basin (bars), compared to the global mean (lines). Blue and red horizontal lines denote the POD and FAR over the globe. c–d, same as a–b, except for the number of hits (blue bars), misses (green bars), and false alarms (red bars) detected by the UZ (c) and OWZ (d) trackers.

342

343

344

345

346

347

348

349

350

For each basin, the distributions of the POD of TCs (Figs. 3a–b) and the number of hits (Figs. 3c–d) between the two trackers show high similarities. Specifically, both trackers report higher POD values in the SI (90% for OWZ tracker, 83% for UZ tracker), WNP (86% for OWZ tracker, 77% for UZ tracker), and SP (84% for OWZ tracker, 68% for UZ tracker), followed by the NI (78% for OWZ tracker, 68% for UZ tracker). Lower POD values are observed in the NATL (62% for OWZ tracker, 48% for UZ tracker) and the ENP (52% for both OWZ and UZ trackers). Similarly, the largest number of TC hits is observed in the WNP (824 for OWZ tracker, 733 for UZ tracker) and SI (543 for OWZ tracker, 503 for UZ tracker), followed by the ENP, SP and NATL, each with approximately 200–300 TCs, and the NI with fewer than 200 TCs.

351

352

353

354

355

356

357

358

359

360

361

The FAR of TCs (Figs. 3a–b), and the number of false alarms (FAs) and misses (Figs. 3c–d) vary between the two trackers. The UZ tracker exhibits FARs below 15% across all basins except the NI. Notably, in the ENP and NATL, the FAR of TCs is below the global average of 7%, with the number of FAs fewer than 20. The OWZ tracker shows a FAR close to the global average (15%) in the WNP and SI, while in the ENP, SP, and NATL, the FAR values range between 15% and 20%. In the NI, however, the two trackers show a relatively higher FAR and more FAs compared to other basins. In terms of missed TC detections, both trackers show relatively few misses, less than 120, in the SP, NI, and SI basins. On the other hand, misses are higher in the ENP and NATL. Overall, the UZ tracker consistently shows a higher number of missed TCs across all basins than the OWZ tracker. This is particularly evident in the WNP and SI, the two basins that account for nearly two-thirds of global TC activity, where the OWZ tracker exhibits fewer missed TC detections (Fig. 3d). Supplementary Sect. S2.1 provides further



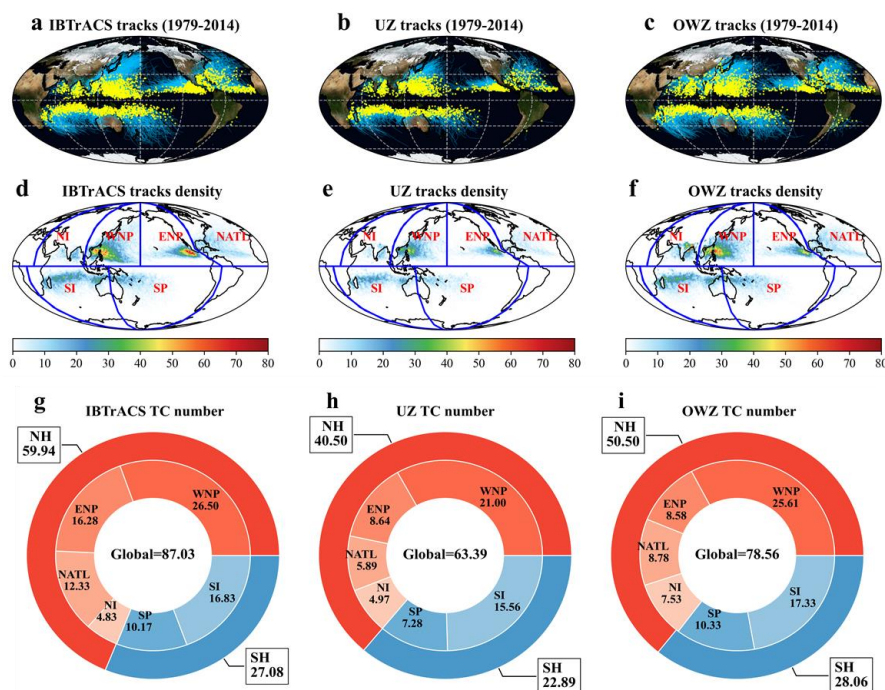
362 explanations of the high FAR of TCs observed in the NI, the higher number of missed TCs in the ENP
363 and NATL (Supplementary Fig. S2).

364 Overall, the accuracies of TC detection by the two tracking algorithms, especially that by the OWZ
365 tracker, have reached the accuracy reported by recent works that extracted TCs from other modern-era
366 reanalyses, such as the fifth generation ECMWF reanalysis (ERA5) (Supplementary Table S1) (Bourdin
367 et al., 2022; Murakami, 2014). This confirms the effectiveness of both trackers in detecting and tracking
368 the majority of TCs from the 20CRv3.

369 3.3 Climatology of TC activity

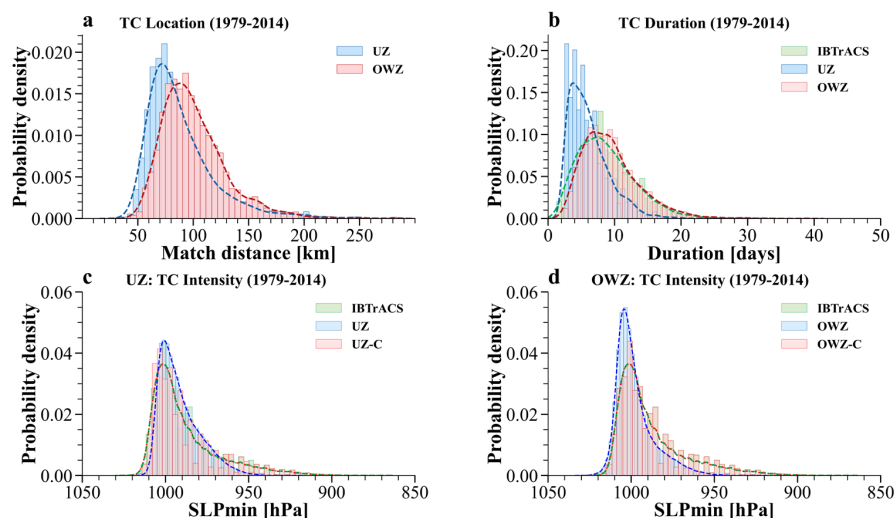
370 Since our target of constructing the RGTracks-20C is to aid the community in studying the response
371 of TCs to climate change, we will focus on the ability of the RGTracks-20C to capture the climatology
372 and long-term variability of TC activity in the following sections.

373 In terms of climatology, the RGTracks-20C is able to capture the major spatial patterns of TC genesis
374 locations and track density over most ocean basins (Figs. 4a–f), indicating its effectiveness in reproducing
375 the spatial distribution of historically observed TCs. The annual mean TC numbers in most ocean basins
376 detected by the UZ and OWZ trackers are consistent with observations (Figs. 4g–i). The OWZ tracker
377 especially captures the observed annual mean TC number in the NWP, SI, and SP well, with discrepancies
378 ranging from -0.48 to 0.89 . Notably, the UZ tracker also accurately estimates observed annual mean TC
379 number in the NI, demonstrating a relatively small error (4.83 versus 4.97) between the two. However,
380 the UZ and OWZ trackers estimate the annual mean number of TCs to be 63.39 and 78.56 , respectively
381 (Figs. 4h–i), which are relatively lower than the observed values (87.03 , Fig. 4g). The main reason for
382 the global underestimation compared to IBTrACS is the discrepancies in the ENP and NATL, of which
383 the reasons are discussed in Supplementary Sects. S2.1–2.2. Despite the underestimations in individual
384 basins, the overall TC detection rates resemble previous publications that aimed to extract TCs from
385 higher-quality reanalyses (Bourdin et al., 2022; Murakami, 2014). This result verifies the RGTracks-
386 20C's ability to reproduce the climatology of the TC number globally and in most basins.



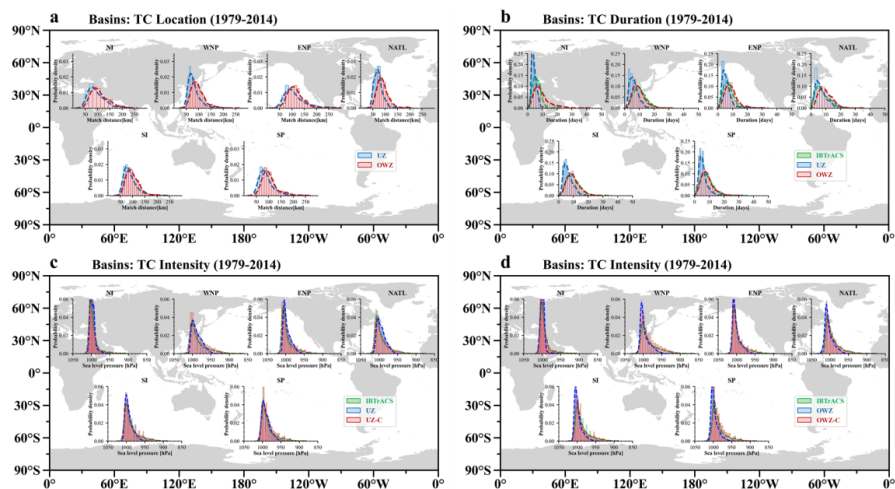
387
 388 **Figure 4: TC genesis locations, tracks, and annual average number from IBTrACS and RGTracks-20C. a–c,**
 389 **TC genesis locations (yellow dots) and tracks (blue lines) from IBTrACS (a), and RGTracks-20C using the UZ**
 390 **(b) and OWZ (c) trackers. d–f, TC tracks density (shading, number of TC occurrence per $1^\circ \times 1^\circ$ latitude-**
 391 **longitude grid box, 1979–2014) from IBTrACS (d), and RGTracks-20C using the UZ (e) and OWZ (f) trackers.**
 392 **g–i, mean number of TCs per year globally and for the six basins from IBTrACS (g), and RGTracks-20C using**
 393 **the UZ (h) and OWZ (i) trackers.**

394
 395 We further evaluate the accuracies of detected TC tracks in the RGTracks-20C by comparing the
 396 arc length of TC tracks between RGTracks-20C and IBTrACS. Results indicate that the global TC
 397 location errors range from 10 to 300 km, with the majority between 50–100 km for the UZ tracker and
 398 75–125 km for the OWZ tracker (Fig. 5a). Additionally, the peak errors for both trackers are below 100
 399 km, with the UZ and OWZ trackers showing peak values of approximately 75 km and 95 km, respectively.
 400 These findings are consistent across all basins (Fig. 6a). Given that the lower limit of the average TC
 401 location error expected from the coarse horizontal resolution of the 20CRv3 (1 degree \times 1 degree) is
 402 approximately 100 km, the above-mentioned small mean values of TC location biases confirm that the
 403 RGTracks-20C is capable of reproducing most observed TC tracks and locations.



404
 405 **Figure 5: Distribution of TC characteristics on the IBTrACS and RGTracks-20C. a, Distribution of the mean**
 406 **TC location error from 1979–2014 (unit: km) between IBTrACS and the RGTracks-20C by the UZ (blue) and**
 407 **OWZ (red) algorithms. b, TC duration (unit: days) from 1979 to 2014 in IBTrACS (green) and the RGTracks-**
 408 **20C by the UZ (blue) and OWZ (red) algorithms. c, same as (b), but for TC intensity (SLP_{min} , unit: hPa),**
 409 **based on the UZ tracker, before (blue) and after (red) bias correction. d, same as (c), but for the OWZ tracker.**
 410 **(UZ: UZ tracker, OWZ: OWZ tracker. UZ-C and OWZ-C represent bias-corrected results for the UZ and**
 411 **OWZ trackers, respectively.)**

412



413
 414 **Figure 6: As in Fig. 5, but for six individual basins.**
 415

416 The duration and intensity of TCs are crucial in climate change research, as global warming may
 417 lead to stronger and longer-lasting TCs (Knutson et al., 2010). However, observational limitations make
 418 these findings more controversial compared to those on TC frequency (Knutson et al., 2010). The



419 RGTracks-20C provides additional support in resolving this controversy. Based on the IBTrACS, the
420 majority of observed TCs globally last fewer than 20 days, with a peak around 8 days (Fig. 5b).
421 Evaluation results (Fig. 5b and Supplementary Fig. S4) show that TCs detected by the OWZ tracker
422 exhibit durations that are close to the observations, and accurately reproduce the TC duration distribution
423 with a peak of 8 days. However, bias is found in the durations of those detected by the UZ tracker, which
424 exhibits a duration peak of approximately 5 days. This is mainly due to the dynamics-based OWZ tracker
425 having the ability to detect storms early in their development (Bell et al., 2018; Bourdin et al., 2022)
426 (Supplementary Fig. S4), while the UZ tracker easily misses weak and short storms (Supplementary Figs.
427 S1a, c) from the 20CRv3 (Bourdin et al., 2022; Tory et al., 2013; Zarzycki and Ullrich, 2017)
428 (Supplementary Sect. S2.3). Similar results are obtained in different basins (Fig. 6b), thus, it is
429 recommended to use the OWZ output when analyzing the durations of TCs.

430 For TC intensity, given the relatively considerable uncertainty in $WIND_{max}$ compared to SLP_{min} in
431 both reanalyses and IBTrACS (see Methods) (Bourdin et al., 2022; Chavas et al., 2017; Knapp et al.,
432 2010; Knutson et al., 2015; Schreck et al., 2014), this study exclusively utilizes SLP_{min} to evaluate the
433 capability of RGTracks-20C in representing the intensity of TCs. According to IBTrACS (Figs. 5c–d),
434 the intensity of TCs is mainly distributed between 900 and 1020 hPa , peaking around 1000 hPa , with a
435 long tail on the lower SLP_{min} side. In contrast, the SLP_{min} in RGTracks-20C is mainly distributed in the
436 range of 950 – 1020 hPa , with peaks at 1000 hPa and 1005 hPa for the UZ (Fig. 5c) and OWZ (Fig. 5d)
437 trackers, respectively. This suggests that the 20CRv3 generally underestimates the TC intensity
438 (Supplementary Fig. 2a), which, as expected, is primarily because the relatively low spatial resolution of
439 the reanalysis may cause smoothing effects on the sea level pressure field. Apart from spatial resolution,
440 the model's dependence on parameterization processes, along with other factors, may also influence its
441 ability to reproduce TC intensity in the reanalysis (Aarons et al., 2021; Hodges et al., 2017; Malakar et
442 al., 2020).

443 To address this issue, an intensity bias correction was implemented using quantile mapping bias
444 correction (see Methods) (Zhao and Held, 2010). After intensity correction, the TC intensity distribution
445 in RGTracks-20C is more consistent with IBTrACS (Figs. 5c–d, and Supplementary Fig. 2b), especially
446 in terms of peak positions, and accurately reproduces the skewed distribution of TC intensity. In particular,
447 the RGTracks-20C reproduces TC intensity values with SLP_{min} below 940 hPa , which were not found
448 before the intensity bias correction. This consistency is observed not only on a global scale but also across
449 various basins (Figs. 6c–d).

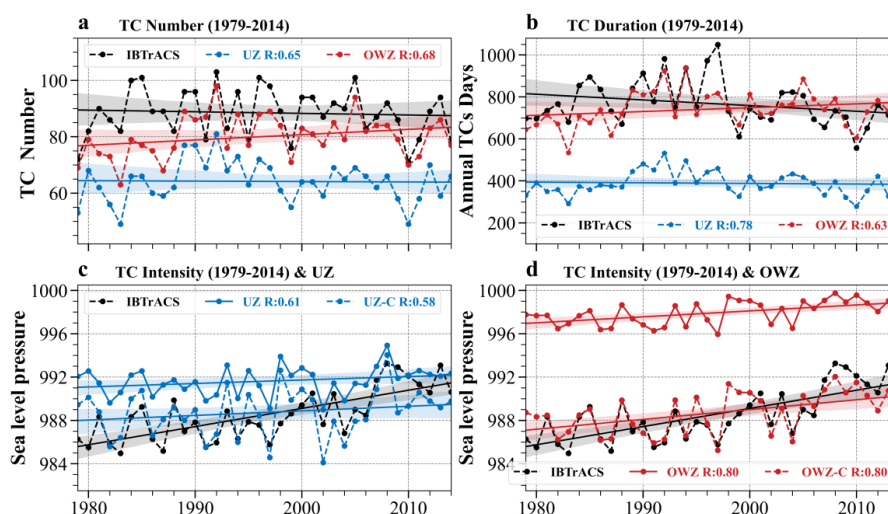
450 3.4 Long-term variability of TC activity

451 This section evaluates the long-term variability of TC activity in the RGTracks-20C by comparing
452 it with the IBTrACS from 1979 to 2014.

453 Firstly, the RGTracks-20C is able to capture the observed interannual variability of global TC
454 number (Fig. 7a), as indicated by the significant correlations between the TC counts derived from the UZ
455 and OWZ trackers and observations, with correlation coefficients of 0.65 and 0.68 (in the following
456 context, all correlations are significant at the 99% confidence level unless otherwise specified),
457 respectively. This is also true for individual basins (Figs. 8a, d), with the correlation coefficients
458 exceeding 0.70 in most basins. Among the six basins, the highest correlation is observed in the NATL,

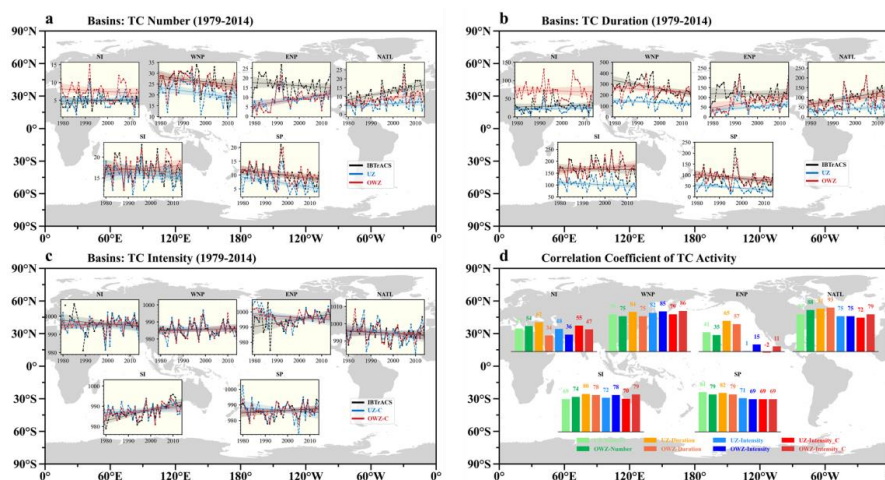


459 where the correlation coefficient for the OWZ tracker reaches 0.88 (0.79 for the UZ tracker). Subsequent
 460 regions with notable correlations include the WNP (0.75 for OWZ tracker, 0.79 for UZ tracker), SP (0.79
 461 for OWZ tracker, 0.84 for UZ tracker), and SI (0.74 for OWZ tracker, 0.69 for UZ tracker). However,
 462 the correlation coefficients are relatively lower in the ENP and NI (Supplementary Table S2), of which
 463 the reasons are discussed in Supplementary Sect. S2.2. Notably, the long-term trends in the number of
 464 TCs recorded by the two datasets are consistent globally and across most of the ocean basins
 465 (Supplementary Table S4).



466
 467 **Figure 7: Time series of globally TC activities from IBTrACS and RGTracks-20C during the periods 1979-**
 468 **2014. TC activities are from the IBTrACS and RGTracks-20C using UZ (blue), and OWZ (red) trackers. a,**
 469 **TC number. b, TC days (unit: days). c, TC intensity in SLP_{min} (unit: hPa) in IBTrACS (black) and RGTracks-**
 470 **20C using UZ tracker before (blue solid line) and after (blue dotted line) bias correction. d, same as (c),**
 471 **except for TC intensity in SLP_{min} (unit: hPa) in IBTrACS (black) and RGTracks-20C using OWZ tracker before**
 472 **(red solid line) and after (red dotted line) bias correction. Shaded areas are the two-sided interval of the linear**
 473 **trend at the 95% confidence level. Straight lines are the linear regression. The correlation coefficients (R)**
 474 **between from IBTrACS and RGTracks-20C are marked in the figure legends. All correlation coefficients are**
 475 **statistically significant at the 99% confidence level.**

476



477
 478 **Figure 8:** As in Fig. 7, but for six basins. a, TC number. b, TC days (unit: days). c, TC intensity in SLP_{min}
 479 (unit: hPa) in IBTrACS (black) and RGTracks-20C (after bias correction) using UZ (blue) and OWZ (red)
 480 trackers. d, the correlation coefficients (R) between the from IBTrACS and RGTracks-20C. Note*: The R
 481 values for TC number and TC intensity are not statistically significant at the 99% confidence level in the NI
 482 and ENP. For TC days, the R value is not statistically significant only in the NI. The R values need to be
 483 divided by 100.

484
 485 TC days, an important metric, encompasses both TC frequency and lifespan (Bell et al., 2018). The
 486 RGTracks-20C is able to reproduce the interannual variability of TC days, which is consistent with that
 487 in IBTrACS (Fig. 7b), with high correlation coefficients of 0.78 and 0.63 for the UZ and OWZ trackers,
 488 respectively. Moreover, these results are further confirmed across basins (Fig. 8b), with correlation
 489 coefficients generally exceeding 0.75. In particular, in the NATL, the correlation coefficient exceeds 0.90
 490 (UZ tracker: 0.93, OWZ tracker: 0.91), followed by the SP (UZ tracker: 0.82, OWZ tracker: 0.79), the SI
 491 (UZ tracker: 0.80, OWZ tracker: 0.78) and the WNP (UZ tracker: 0.84, OWZ tracker: 0.75). However,
 492 being influenced by the observation biases, the correlation coefficients for TC days are also relatively
 493 low in the ENP and NI (see Supplementary Table S2). Nevertheless, the above results indicate that the
 494 RGTracks-20C provides a satisfactory representation of the interannual and long-term variability
 495 (Supplementary Sect. S2.4, Table S4) of the TC days globally and across most of the ocean basins.

496 In addition, the global TC intensity series based on RGTracks-20C significantly correlates with that
 497 based on IBTrACS, with correlation coefficients of 0.61 and 0.80 for the UZ (Fig. 7c) and OWZ (Fig.
 498 7d) trackers, respectively. This indicates that the TC intensity (SLP_{min}) in RGTracks-20C effectively
 499 captures the observed interannual variability. Most basins further validate these results (Fig. 8d). The
 500 highest correlation coefficients are observed in the WNP, exceeding 0.80 (UZ tracker: 0.82, OWZ tracker:
 501 0.85). Following closely are NATL (UZ tracker: 0.75, OWZ tracker: 0.75) and SI (UZ tracker: 0.72,
 502 OWZ tracker: 0.78), while SP (UZ tracker: 0.71, OWZ tracker: 0.69) also demonstrates correlation
 503 coefficients of around 0.70.

504 The 20CRv3 tends to underestimate the TC intensities, due to its coarse resolution, which suggests
 505 the need of a bias correction process during the production of the RGTracks-20C (see Methods). By

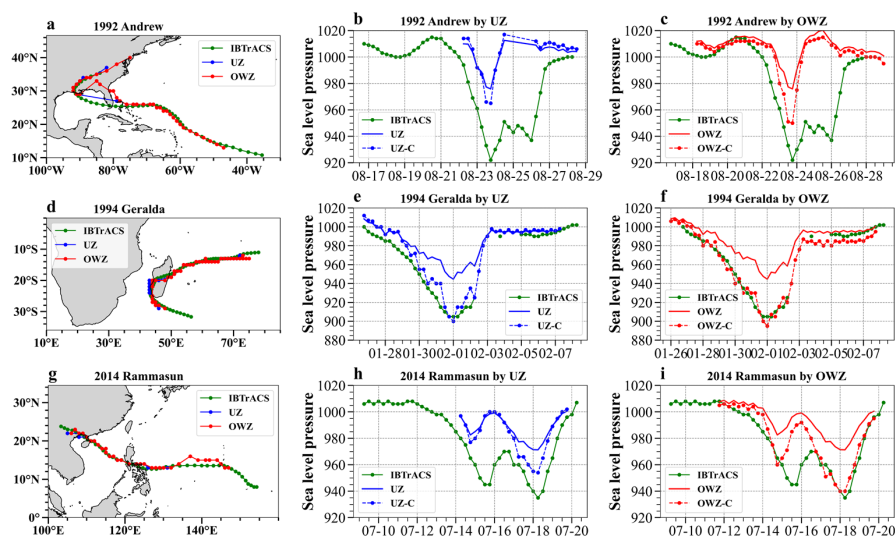


506 performing intensity bias corrections to the detected TCs, the TC intensity (SLP_{min}) in RGTracks-20C
507 exhibits interannual and long-term variations that are more consistent with the observations (Figs. 7c–d,
508 and Supplementary Fig. 2 and Tables S2, S4), especially in the WNP, NATL, and SI basins (Figs. 8c–d).
509 These results indicate that the RGTracks-20C can reasonably capture the interannual variability and
510 trends (Supplementary Sect. S2.4 and Table S4) of TC intensity globally and across most basins.
511 Discrepancies in the interannual variability of TC intensity between the RGTracks-20C and IBTrACS
512 are also noted over ENP and NI, similar to the above findings on TC number and days (Supplementary
513 Sect. S2.2 and Tables S6–S7).

514 **3.5 Key strengths of the RGTracks-20C**

515 The above evaluation analyses confirm that the RGTracks-20C effectively captures both the
516 climatology and long-term variability of TC activity across global and major oceanic basins. In this
517 section, we discuss the key strengths of the RGTracks-20C, specifically its capacity to reconstruct track
518 and intensity information of early-year TCs that may not be included in the observed data records. Such
519 an advantage of the RGTracks-20C could benefit research about how climate change has affected TCs
520 over the past century.

521 Before digging into early-year TCs, we first demonstrate the RGTracks-20C's accuracy in
522 reproducing specific TCs by making comparisons with observations. Three representative TCs that
523 caused significant human casualties and economic losses in the NATL, SI, and WNP are analyzed here:
524 Hurricane 'Andrew' in 1992 (Pimm et al., 1994) (Figs. 9a–c), TC 'Geralda' in 1994 (Hoarau et al., 2012)
525 (Figs. 9d–f), and Super Typhoon 'Rammasun' in 2014 (Zhang et al., 2017) (Figs. 9h–i). Compared with
526 IBTrACS, the RGTracks-20C performs exceptionally well in representing the track and duration of these
527 TCs. However, some discrepancies were observed during landfall (Fig. 9a), possibly due to complex
528 topography and TC size, which were not captured by the low-resolution 20CRv3. While the 20CRv3
529 tends to underestimate the intensity of TCs, the corrected intensity in the RGTracks-20C is highly
530 consistent with observations and accurately captures the temporal evolutions of TC intensities. This
531 evidence confirms RGTracks-20C's ability to capture not only the climatology and variability of TC
532 activity, but also the detailed information on specific TC events.



533

534

535

536

537

538

539

540

541

542

543

544

545

546

547

548

549

550

551

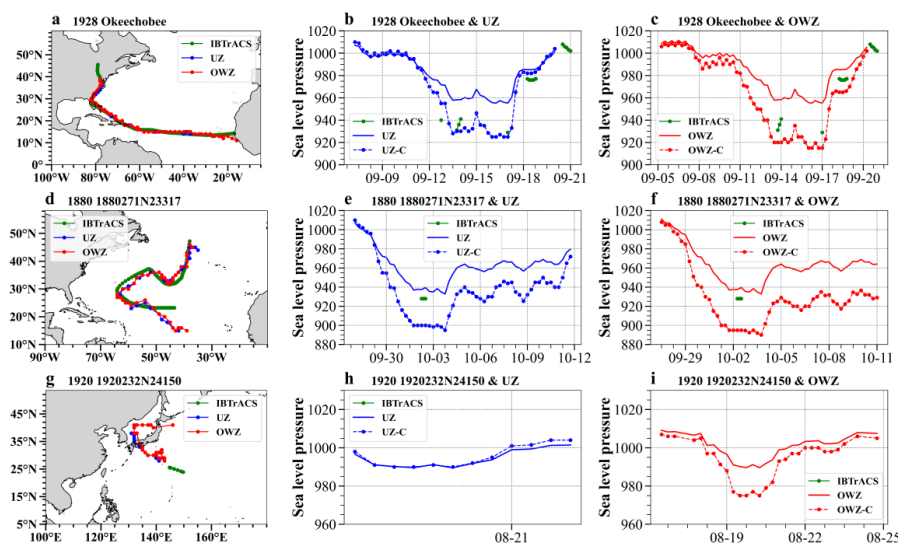
552

553

554

Figure 9: The historical tracks and intensity records of individual tropical cyclones in the IBTrACS and RGTracks-20C. a–c, Track (a) and intensity (SLP_{min} , unit: hPa. b: UZ tracker, c: OWZ tracker) of Hurricane “Andrew”. d–f, same as a–c, but for track (d) and intensity (SLP_{min} , unit: hPa. e: UZ tracker, f: OWZ tracker) of tropical cyclone “Geralda”. g–i, same as a–c, track (g) and intensity (SLP_{min} , unit: hPa. h: UZ tracker, i: OWZ tracker) of Super typhoon “Rammasun”. Green, blue, and red lines denote results based on the IBTrACS, UZ tracker, and OWZ tracker, respectively. The UZ-C (blue dotted dashed line) and OWZ-C (red dotted dashed line) indicate after intensity bias correction.

Prior to the satellite era, limitations in observation systems often led to incomplete records of early TCs, particularly for TC intensity. An example is hurricane Okeechobee in 1928, which was one of the deadliest to hit the United States in the early 20th century. Hurricane Okeechobee was recorded in the IBTrACS (Blake et al., 2011; Mitchell, 1928) (Supplementary Sect. S3.1). However, during Okeechobee’s lifetime, there were only 16 time points of the TC intensity that were recorded when it passed the Lesser Antilles and Puerto Rico, and made landfall in the United States (Figs. 10a–c, Supplementary Fig. S5 and Table S8). Similar missing data are common in the IBTrACS records of early TCs, especially when the TCs were located over the ocean (Figs. 10d–f). Moreover, the problem of missing TC intensity records is especially evident in other basins (Supplementary Table S3). For instance, Typhoon No. 8, which made landfall and caused serious damage in Japan (see Supplementary Sect. S3.2), has only track records in the IBTrACS, but with intensity information missing (Figs. 10g–i). In such cases, taking advantage of the 20CRv3, the RGTracks-20C addresses these deficiencies by filling in these gaps, substantially enhancing the completeness of early TC intensity records.



555
 556 **Figure 10:** As in Fig. 9, but for Hurricane “Okeechobee” (a–c), Hurricane ‘1880271N23317’ (d–f), typhoon
 557 ‘192023N24150’ (g–i).

558
 559 In addition, not only is the TC intensity missing, but the track records in the IBTrACS may also be
 560 incomplete, such as the above-mentioned Typhoon No.8 in 1920 (Fig. 10g), despite the existence of
 561 historical observation records (see Supplementary Sect. S3.2). In this case, the RGTracks-20C not only
 562 provides the missing TC intensity but also fills gaps in IBTrACS during the latter stages of the typhoon's
 563 development, especially during the landfall phase (Fig. 10g and Supplementary Figs. S6–8). Moreover,
 564 prior to the satellite era, the RGTracks-20C often reports a higher number of TCs than the IBTrACS,
 565 particularly from the early to mid-20th century (Supplementary Fig. S10), which suggests that the
 566 RGTracks-20C is also able to detect historical TCs not being recorded in the IBTrACS. These findings
 567 demonstrate that the RGTracks-20C can compensate for the incomplete TC track records in the IBTrACS,
 568 especially for those in the pre-satellite era.

569 To evaluate the accuracy of early TC records provided by RGTracks-20C, we take the 1928
 570 Okeechobee hurricane as a case study. The RGTracks-20C nearly fully reproduces the hurricane's
 571 lifespans as recorded in IBTrACS, with the OWZ tracker performing exceptionally well, differing by
 572 only one day from the IBTrACS record. Okeechobee's latitude and longitude variations in the RGTracks-
 573 20C are highly consistent with those in the IBTrACS, with a positional bias within ± 1 degree (Fig. 10a
 574 and Supplementary Fig. S5). By comparing Okeechobee's intensity in RGTracks-20C with observational
 575 data, we find that the RGTracks-20C reliably reproduces Okeechobee's intensity and its variations (Figs.
 576 10b–c and Supplementary Table S8). For instance, as the hurricane passed over Guadeloupe, IBTrACS
 577 recorded a SLP_{min} of 940 hPa, which is closely matched by RGTracks-20C (UZ tracker: 955 hPa; OWZ
 578 tracker: 940 hPa). Moreover, the RGTracks-20C captures the weakening and re-intensification of the
 579 hurricane between Puerto Rico and its landfall in Florida, where the IBTrACS lacks intensity records,
 580 demonstrating the RGTracks-20C's reliability in representing intensity changes (Supplementary Sect.
 581 S3.1).



582 **4. Usage notes**

583 In this study, we introduce the RGTracks-20C, a century-long reanalysis-based historical global TC
584 dataset. Statistical evaluations and case studies confirm RGTracks-20C's reliability in capturing the
585 climatology and interannual variability of observed TC activity on both global and regional scales in the
586 modern satellite era. A major key strength of the RGTracks-20C is its ability to fill the missing intensity
587 or location records of observed TCs in early years.

588 As documented in prior studies, biases are unavoidable when extracting TCs from reanalyses due
589 to the data quality of reanalyses and the limitations of TC trackers. Some usage notes and cautionary
590 remarks are listed in this section to assist readers in understanding or using the RGTracks-20C.

591 (1) Due to model resolution and parameterization, TC intensity detected directly from the 20CRv3
592 is underrepresented compared to observations. To address this issue in the RGTracks-20C, we corrected
593 the biases using a simple quantile mapping method, assuming that systematic biases primarily cause the
594 TC intensity errors from 20CRv3. While this is generally true, the quantile mapping correction did not
595 account for other factors that may also affect TC intensity biases. The inherent challenges in modeling
596 weaker TCs in 20CRv3, which are largely attributed to the limitations of resolution and parameterization
597 of subgrid-scale processes in numerical models, often result in lower detection rates for tropical
598 depressions and weaker tropical storms (e.g., Category 1) (Hodges et al., 2017). This can be improved
599 with more advanced correction approaches of TC intensity in the future.

600 (2) Discrepancies between the RGTracks-20C and IBTrACS should not be solely attributed to errors
601 in RGTracks-20C, as limitations in IBTrACS may also influence the evaluation results. For example, the
602 classification of TC often relies on forecasters' subjective judgment, which affects whether these systems
603 are included in best track datasets (Torn and Snyder, 2012). Additionally, differences in observation
604 start times and data sources across basins (Supplementary Table S3) can introduce uncertainties in the
605 IBTrACS data (Chan et al., 2022b). For example, the RGTracks-20C shows relatively large discrepancies
606 with observations in the ENP (Supplementary Sect. S2.2), which may be attributed to the biases of
607 IBTrACS prior to 1988. Similar issues exist for the NI basin. When limiting the study periods to 1988–
608 2014 for the ENP and 1990–2014 for the NI, the RGTracks-20C exhibits good consistency with IBTrACS
609 in TC activity trends, and the correlation significantly improves (Supplementary Fig. S3 and Tables S2,
610 S5). These suggest that the reliability of observational data has been changing over time and may serve
611 as a factor affecting the comparison results between the RGTracks-20C and observational records.
612 Detailed analyses on these two basins can be found in Supplementary Sect. S2.2.

613 (3) Currently, there are no perfect algorithms for tracking TCs from reanalyses. Although the TC
614 trackers employed in the RGTracks-20C (UZ and OWZ) are two widely recognized algorithms, they were
615 built with different properties and have different limitations. The above evaluation analyses show that the
616 OWZ tracker is closer to the observations in terms of TC number and TC days (Bourdin et al., 2022),
617 while the UZ tracker produces tracks with a shorter duration than the observations, which is mainly
618 related to its physically based tracker intensity threshold (Horn et al., 2014). However, the UZ has a lower
619 FAR, suggesting that it has an advantage in recognizing real TCs and is less likely to misclassify other
620 weather systems as TCs. Generally, since the OWZ tracker demonstrates overall higher stability in
621 detecting TCs, it is recommended to primarily utilize the OWZ tracker results in most cases, with the UZ



622 tracker as a supplementary reference for analyses. In addition, in the production of the RGTracks-20C,
623 globally identical thresholds were used in the TC tracking procedure. However, given the differences in
624 structure and behavior of TCs in different basins and the influence of different meteorological systems
625 and topography, the use of a globally identical tracker may affect the accuracies of TC detection in
626 specific regions (Fu et al., 2021; Raavi and Walsh, 2020a, b). This suggests the need for further
627 improvements in the TC tracking approaches.

628 (4) The assimilation of SLP_{min} from IBTrACS into the 20CRv3 may lead to into the 20CRv3 may
629 lead to another limitation. As discussed in Supplementary Sect. S4, the RGTracks-20C exhibits consistent
630 trends and variations with IBTrACS from 1850 to 2014 (Supplementary Fig. S10). In particular, the
631 growth trends in TC numbers from both datasets during the mid-20th century are almost identical,
632 primarily resulting from the artificial increase in TC detection associated with advancements in
633 observational technologies. considering that RGTracks-20C currently uses the ensemble mean field of
634 20CRv3 as input data, which inherently attenuates the intensity and features of extreme events and
635 introduces smoothing effects. In addition, RGTracks-20C currently uses the ensemble mean field of
636 20CRv3 as input data, which further affects this similarity by inherently weakening the intensity and
637 character of extreme events and introducing smoothing effects (Emanuel, 2024). On the other hand, the
638 assimilation of IBTrACS data has, to some extent, also improved 20CRv3's representation of TC intensity
639 and structure, enabling TC tracker to more effectively detect and identify TCs that actually occurred
640 (Slivinski et al., 2019, 2021). For example, the typhoon that made landfall in Japan in 1920 (Fig. 10g).
641 Nevertheless, this limitation implies that the RGTracks-20C fails to capture the realistic number of TCs
642 in early years, and suggests the need to employ individual members for TC detections (Emanuel, 2024).

643 The above factors will be thoroughly considered and addressed in the future versions of RGTracks-
644 20C to enhance its accuracy and applicability. In the next version of RGTracks-20C, a few improvements
645 will be included: (1) We detect TCs separately from all 80 ensemble members of the 20CRv3, in order to
646 avoid the smoothing effects caused by the ensemble mean of reanalyses (Emanuel, 2024); (2) we will
647 calibrate algorithm thresholds according to TC characteristics in different ocean basins; (3) more TC
648 tracking algorithms will be included to address the uncertainty of the TC track data (Flaounas et al., 2023).

649 5. Data Availability

650 The RGTracks-20C is publicly available at <https://doi.org/10.5281/zenodo.14411917> (Ye et al., 2024).
651 The Other datasets utilized in this study are available: the IBTrACS at <https://www.ncdc.noaa.gov/ibtracs/>;
652 and the 20CRv3 at <https://portal.nersc.gov/archive/home/projects/incite11/www/> (Slivinski et al., 2019).
653 Historical weather chart of the 1920 typhoon that made landfall in Japan from
654 <http://agora.ex.nii.ac.jp/cgi-bin/weather-chart/calendar.pl?year=1920&month=8&lang=en&type=as>.

655 6. Code Availability

656 Bourdin (2022a) provided the code for the UZ and OWZ algorithms, which are available at
657 <https://doi.org/10.5281/zenodo.6424432>. TempestExtremes can be downloaded from
658 <https://climate.ucdavis.edu/tempestextremes.php>, and version 1.5.2 is used for this study.



659 **7. Conclusion**

660 In this study, we introduce the RGTracks-20C, a century-long reanalysis-based historical global TC
661 dataset. Statistical evaluations and case studies confirm its reliability in capturing the climatology and
662 interannual variability of observed TC activity on both global and regional scales. A major key strength
663 of the RGTracks-20C is its ability to fill the missing intensity and location records of observed TCs in
664 early years. This dataset provides a reliable alternative for researchers to study the long-term variability
665 of TC characteristics, which will help us to better understand changes and trends in historical TC activity,
666 as well as their relationship with climate change.

667 This knowledge is crucial for protecting vulnerable coastal areas and mitigating TC-related risks in
668 the future climate change. As the first version, the RGTracks-20C has limitations, which may arise from
669 the reanalysis assimilation process and the threshold settings in the TC tracker. Future versions will
670 further address these issues, refining the dataset to improve accuracy and broaden applicability.

671 **Competing interests**

672 The authors declare no competing interests.

673 **Author contributions**

674 G.Y.: methodology, formal analysis, data curation, visualization, writing—original draft,
675 writing—review and editing, software;

676 J.C.H.L.: conceptualization, methodology, formal analysis, writing—original draft, writing—
677 review and editing, funding acquisition;

678 W.D.: writing—review and editing, supervision, funding acquisition;

679 J.X., W.L. and W.Q.: writing—review and editing;

680 B.Z.: conceptualization, supervision, methodology, formal analysis, writing—review and editing,
681 funding acquisition.

682 **Acknowledgements**

683 The authors sincerely thank Dr. Stella Bourdin from the Laboratoire des Sciences du Climat et de
684 l'Environnement, Institut Pierre Simon Laplace (LSCE-IPSL), Gif-sur-Yvette, for her invaluable
685 assistance and guidance on the TC trackers. The authors are very grateful to Dr. Jennifer Gahtan from
686 NOAA's National Center for Environmental Information for providing information about the starting
687 years of the minimum central pressure in the IBTrACS.

688 This study is primarily supported by the National Natural Science Foundation of China (Grant No.
689 U21A6001). G.Y. and W.D. are also supported by the Southern Marine Science and Engineering
690 Guangdong Laboratory (No. SML2023SP208). G.Y., J.C.H.L., J.X., W.L., W.Q., and B.Z. are supported
691 by the Guangdong Province Introduction of Innovative R&D Team Project China (2019ZT08G669). J.X.
692 is supported by the National Natural Science Foundation of China (42130605). J.C.H.L. is supported by



693 the National Natural Science Foundation of China (42405038) and the Guangdong Basic and Applied
694 Basic Research Foundation (2020A1515110275).

695 **Author contributions**

696 G.Y.: methodology, formal analysis, data curation, visualization, writing—original draft,
697 writing—review and editing, software;
698 J.C.H.L.: conceptualization, methodology, formal analysis, writing—original draft, writing—
699 review and editing, funding acquisition;
700 W.D.: writing—review and editing, supervision, funding acquisition;
701 J.X., W.L. and W.Q.: writing—review and editing;
702 B.Z.: conceptualization, supervision, methodology, formal analysis, writing—review and editing,
703 funding acquisition.
704
705
706

707 **References**

- 708 Aarons, Z. S., Camargo, S. J., Strong, J. D. O., and Murakami, H.: Tropical Cyclone
709 Characteristics in the MERRA-2 Reanalysis and AMIP Simulations, *Earth and Space*
710 *Science*, 8, e2020EA001415, <https://doi.org/10.1029/2020EA001415>, 2021.
- 711 Bell, S. S., Chand, S. S., Tory, K. J., and Turville, C.: Statistical Assessment of the OWZ
712 Tropical Cyclone Tracking Scheme in ERA-Interim, *Journal of Climate*, 31, 2217–2232,
713 <https://doi.org/10.1175/JCLI-D-17-0548.1>, 2018.
- 714 Bhatia, K. T., Vecchi, G. A., Knutson, T. R., Murakami, H., Kossin, J., Dixon, K. W., and
715 Whitlock, C. E.: Recent increases in tropical cyclone intensification rates, *Nat Commun*,
716 10, 635, <https://doi.org/10.1038/s41467-019-08471-z>, 2019.
- 717 Blake, E. S., Landsea, C., and Gibney, E. J.: The deadliest, costliest, and most intense United
718 States tropical cyclones from 1851 to 2010 (and other frequently requested hurricane
719 facts), 2011.
- 720 Bloemendaal, N., de Moel, H., Martinez, A. B., Muis, S., Haigh, I. D., van der Wiel, K.,
721 Haarsma, R. J., Ward, P. J., Roberts, M. J., Dullaart, J. C. M., and Aerts, J. C. J. H.: A
722 globally consistent local-scale assessment of future tropical cyclone risk, *Science*
723 *Advances*, 8, eabm8438, <https://doi.org/10.1126/sciadv.abm8438>, 2022.
- 724 Bourdin, S., Fromang, S., Dulac, W., Cattiaux, J., and Chauvin, F.: Intercomparison of four
725 algorithms for detecting tropical cyclones using ERA5, *Geoscientific Model*
726 *Development*, 15, 6759–6786, <https://doi.org/10.5194/gmd-15-6759-2022>.



- 727 Chan, J. C. L.: Frequency and Intensity of Landfalling Tropical Cyclones in East Asia: Past
728 Variations and Future Projections, *Meteorology*, 2, 171–190,
729 <https://doi.org/10.3390/meteorology2020012>, 2023.
- 730 Chan, K. T. F.: Are global tropical cyclones moving slower in a warming climate? *Environ.*
731 *Res. Lett.*, 14, 104015, <https://doi.org/10.1088/1748-9326/ab4031>, 2019.
- 732 Chan, K. T. F., Zhang, K., Wu, Y., and Chan, J. C. L.: Publisher Correction: Landfalling
733 hurricane track modes and decay, *Nature*, 608, E14–E14, [https://doi.org/10.1038/s41586-](https://doi.org/10.1038/s41586-022-05078-1)
734 [022-05078-1](https://doi.org/10.1038/s41586-022-05078-1), 2022a.
- 735 Chan, K. T. F., Chan, J. C. L., Zhang, K., and Wu, Y.: Uncertainties in tropical cyclone landfall
736 decay, *npj Clim Atmos Sci*, 5, 1–8, <https://doi.org/10.1038/s41612-022-00320-z>, 2022b.
- 737 Chand, S. S., Walsh, K. J. E., Camargo, S. J., Kossin, J. P., Tory, K. J., Wehner, M. F., Chan, J.
738 C. L., Klotzbach, P. J., Dowdy, A. J., Bell, S. S., Ramsay, H. A., and Murakami, H.:
739 Declining tropical cyclone frequency under global warming, *Nat. Clim. Chang.*, 12, 655–
740 661, <https://doi.org/10.1038/s41558-022-01388-4>, 2022.
- 741 Chang, E. K. M. and Guo, Y.: Is the number of North Atlantic tropical cyclones significantly
742 underestimated prior to the availability of satellite observations?, *Geophysical Research*
743 *Letters*, 34, <https://doi.org/10.1029/2007GL030169>, 2007.
- 744 Chavas, D. R., Reed, K. A., and Knaff, J. A.: Physical understanding of the tropical cyclone
745 wind-pressure relationship, *Nat Commun*, 8, 1360, [https://doi.org/10.1038/s41467-017-](https://doi.org/10.1038/s41467-017-01546-9)
746 [01546-9](https://doi.org/10.1038/s41467-017-01546-9), 2017.
- 747 Cid, A., Camus, P., Castanedo, S., Méndez, F. J., and Medina, R.: Global reconstructed daily
748 surge levels from the 20th Century Reanalysis (1871–2010), *Global and Planetary*
749 *Change*, 148, 9–21, <https://doi.org/10.1016/j.gloplacha.2016.11.006>, 2017.
- 750 Compo, G., Slivinski, L., Whitaker, J., Sardeshmukh, P., McColl, C., Brohan, P., Allan, R., Yin,
751 X., Vose, R., Spencer, L., and others: The international surface pressure databank version
752 4, 2019.
- 753 Compo, G. P., Whitaker, J. S., Sardeshmukh, P. D., Matsui, N., Allan, R. J., Yin, X., Gleason,
754 B. E., Vose, R. S., Rutledge, G., Bessemoulin, P., Brönnimann, S., Brunet, M.,
755 Crouthamel, R. I., Grant, A. N., Groisman, P. Y., Jones, P. D., Kruk, M. C., Kruger, A. C.,
756 Marshall, G. J., Maugeri, M., Mok, H. Y., Nordli, Ø., Ross, T. F., Trigo, R. M., Wang, X.
757 L., Woodruff, S. D., and Worley, S. J.: The Twentieth Century Reanalysis Project,
758 *Quarterly Journal of the Royal Meteorological Society*, 137, 1–28,
759 <https://doi.org/10.1002/qj.776>, 2011.
- 760 Cram, T. A., Compo, G. P., Yin, X., Allan, R. J., McColl, C., Vose, R. S., Whitaker, J. S., Matsui,
761 N., Ashcroft, L., Auchmann, R., and others: The international surface pressure databank



- 762 version 2, *Geoscience Data Journal*, 2, 31–46, 2015.
- 763 Dinan, T.: Projected Increases in Hurricane Damage in the United States: The Role of Climate
764 Change and Coastal Development, *Ecological Economics*, 138, 186–198,
765 <https://doi.org/10.1016/j.ecolecon.2017.03.034>, 2017.
- 766 Emanuel, K.: The Hurricane—Climate Connection, *Bulletin of the American Meteorological*
767 *Society*, 89, ES10–ES20, <https://doi.org/10.1175/BAMS-89-5-Emanuel>, 2008.
- 768 Emanuel, K.: Tropical Cyclone Activity Downscaled from NOAA-CIRES Reanalysis, 1908–
769 1958, *Journal of Advances in Modeling Earth Systems*, 2,
770 <https://doi.org/10.3894/JAMES.2010.2.1>, 2010.
- 771 Emanuel, K.: Will Global Warming Make Hurricane Forecasting More Difficult? *Bulletin of*
772 *the American Meteorological Society*, 98, 495–501, [https://doi.org/10.1175/BAMS-D-](https://doi.org/10.1175/BAMS-D-16-0134.1)
773 [16-0134.1](https://doi.org/10.1175/BAMS-D-16-0134.1), 2017.
- 774 Emanuel, K.: 100 Years of Progress in Tropical Cyclone Research, *Meteorological*
775 *Monographs*, 59, 15.1–15.68, [https://doi.org/10.1175/AMSMONOGRAPHS-D-18-](https://doi.org/10.1175/AMSMONOGRAPHS-D-18-0016.1)
776 [0016.1](https://doi.org/10.1175/AMSMONOGRAPHS-D-18-0016.1), 2018.
- 777 Emanuel, K.: Atlantic tropical cyclones downscaled from climate reanalyses show increasing
778 activity over past 150 years, *Nat Commun*, 12, 7027, [https://doi.org/10.1038/s41467-021-](https://doi.org/10.1038/s41467-021-27364-8)
779 [27364-8](https://doi.org/10.1038/s41467-021-27364-8), 2021.
- 780 Emanuel, K.: Limitations of reanalyses for detecting tropical cyclone trends, *Nat. Clim.*
781 *Chang.*, 14, 143–145, <https://doi.org/10.1038/s41558-023-01879-y>, 2024.
- 782 Faranda, D., Messori, G., Bourdin, S., Vrac, M., Thao, S., Riboldi, J., Fromang, S., and Yiou,
783 P.: Correcting biases in tropical cyclone intensities in low-resolution datasets using
784 dynamical systems metrics, *Clim Dyn*, <https://doi.org/10.1007/s00382-023-06794-8>,
785 2023.
- 786 Flaounas, E., Aragão, L., Bernini, L., Dafis, S., Doiteau, B., Flocas, H., Gray, S. L., Karwat,
787 A., Kouroutzoglou, J., Lionello, P., Miglietta, M. M., Pantillon, F., Pasquero, C., Patlakas,
788 P., Picornell, M. Á., Porcù, F., Priestley, M. D. K., Reale, M., Roberts, M. J., Saaroni, H.,
789 Sandler, D., Scoccimarro, E., Sprenger, M., and Ziv, B.: A composite approach to produce
790 reference datasets for extratropical cyclone tracks: application to Mediterranean cyclones,
791 *Weather and Climate Dynamics*, 4, 639–661, <https://doi.org/10.5194/wcd-4-639-2023>,
792 2023.
- 793 Fu, D., Chang, P., Patricola, C. M., Saravanan, R., Liu, X., and Beck, H. E.: Central American
794 mountains inhibit eastern North Pacific seasonal tropical cyclone activity, *Nat Commun*,
795 12, 4422, <https://doi.org/10.1038/s41467-021-24657-w>, 2021.
- 796 Gergis, J., Ashcroft, L., and Whetton, P.: A historical perspective on Australian temperature



- 797 extremes, *Clim Dyn*, 55, 843–868, <https://doi.org/10.1007/s00382-020-05298-z>, 2020.
- 798 Hassanzadeh, P., Lee, C.-Y., Nabizadeh, E., Camargo, S. J., Ma, D., and Yeung, L. Y.: Effects
799 of climate change on the movement of future landfalling Texas tropical cyclones, *Nat*
800 *Commun*, 11, 3319, <https://doi.org/10.1038/s41467-020-17130-7>, 2020.
- 801 Hoarau, K., Bernard, J., and Chalonge, L.: Intense tropical cyclone activities in the northern
802 Indian Ocean, *International Journal of Climatology*, 32, 1935–1945,
803 <https://doi.org/10.1002/joc.2406>, 2012.
- 804 Hodges, K., Cobb, A., and Vidale, P. L.: How Well Are Tropical Cyclones Represented in
805 Reanalysis Datasets? *Journal of Climate*, 30, 5243–5264, [https://doi.org/10.1175/JCLI-](https://doi.org/10.1175/JCLI-D-16-0557.1)
806 [D-16-0557.1](https://doi.org/10.1175/JCLI-D-16-0557.1), 2017.
- 807 Horn, M., Walsh, K., Zhao, M., Camargo, S. J., Scoccimarro, E., Murakami, H., Wang, H.,
808 Ballinger, A., Kumar, A., Shaevitz, D. A., Jonas, J. A., and Oouchi, K.: Tracking Scheme
809 Dependence of Simulated Tropical Cyclone Response to Idealized Climate Simulations,
810 <https://doi.org/10.1175/JCLI-D-14-00200.1>, 2014.
- 811 Kalnay, E., Kanamitsu, M., Kistler, R., Collins, W., Deaven, D., Gandin, L., Iredell, M., Saha,
812 S., White, G., Woollen, J., Zhu, Y., Chelliah, M., Ebisuzaki, W., Higgins, W., Janowiak,
813 J., Mo, K. C., Ropelewski, C., Wang, J., Leetmaa, A., Reynolds, R., Jenne, R., and Joseph,
814 D.: The NCEP/NCAR 40-Year Reanalysis Project, *Bulletin of the American*
815 *Meteorological Society*, 77, 437–472, [https://doi.org/10.1175/1520-](https://doi.org/10.1175/1520-0477(1996)077<0437:TNYRP>2.0.CO;2)
816 [0477\(1996\)077<0437:TNYRP>2.0.CO;2](https://doi.org/10.1175/1520-0477(1996)077<0437:TNYRP>2.0.CO;2), 1996.
- 817 Klotzbach, P. J. and Landsea, C. W.: Extremely Intense Hurricanes: Revisiting Webster et al.
818 (2005) after 10 Years, *Journal of Climate*, 28, 7621–7629, [https://doi.org/10.1175/JCLI-](https://doi.org/10.1175/JCLI-D-15-0188.1)
819 [D-15-0188.1](https://doi.org/10.1175/JCLI-D-15-0188.1), 2015.
- 820 Klotzbach, P. J., Bell, M. M., Bowen, S. G., Gibney, E. J., Knapp, K. R., and Schreck, C. J.:
821 Surface Pressure a More Skillful Predictor of Normalized Hurricane Damage than
822 Maximum Sustained Wind, <https://doi.org/10.1175/BAMS-D-19-0062.1>, 2020.
- 823 Knapp, K. R., Kruk, M. C., Levinson, D. H., Diamond, H. J., and Neumann, C. J.: The
824 International Best Track Archive for Climate Stewardship (IBTrACS): Unifying Tropical
825 Cyclone Data, *Bulletin of the American Meteorological Society*, 91, 363–376,
826 <https://doi.org/10.1175/2009BAMS2755.1>, 2010.
- 827 Knapp, K. R., Diamond, H. J., Kossin, J. P., Kruk, M. C., Schreck, C. J., and others:
828 International best track archive for climate stewardship (IBTrACS) project, version 4,
829 NOAA National Centers for Environmental Information, 10, 2018.
- 830 Knutson, T., Camargo, S. J., Chan, J. C. L., Emanuel, K., Ho, C.-H., Kossin, J., Mohapatra,
831 M., Satoh, M., Sugi, M., Walsh, K., and Wu, L.: Tropical Cyclones and Climate Change



- 832 Assessment: Part I: Detection and Attribution, *Bulletin of the American Meteorological*
833 *Society*, 100, 1987–2007, <https://doi.org/10.1175/BAMS-D-18-0189.1>, 2019.
- 834 Knutson, T., Camargo, S. J., Chan, J. C. L., Emanuel, K., Ho, C.-H., Kossin, J., Mohapatra,
835 M., Satoh, M., Sugi, M., Walsh, K., and Wu, L.: Tropical Cyclones and Climate Change
836 Assessment: Part II: Projected Response to Anthropogenic Warming, *Bulletin of the*
837 *American Meteorological Society*, 101, E303–E322, [https://doi.org/10.1175/BAMS-D-](https://doi.org/10.1175/BAMS-D-18-0194.1)
838 18-0194.1, 2020.
- 839 Knutson, T. R., McBride, J. L., Chan, J., Emanuel, K., Holland, G., Landsea, C., Held, I.,
840 Kossin, J. P., Srivastava, A. K., and Sugi, M.: Tropical cyclones and climate change,
841 *Nature Geosci*, 3, 157–163, <https://doi.org/10.1038/ngeo779>, 2010.
- 842 Knutson, T. R., Sirutis, J. J., Zhao, M., Tuleya, R. E., Bender, M., Vecchi, G. A., Villarini, G.,
843 and Chavas, D.: Global Projections of Intense Tropical Cyclone Activity for the Late
844 Twenty-First Century from Dynamical Downscaling of CMIP5/RCP4.5 Scenarios,
845 *Journal of Climate*, 28, 7203–7224, <https://doi.org/10.1175/JCLI-D-15-0129.1>, 2015.
- 846 Kossin, J. P., Knapp, K. R., Olander, T. L., and Velden, C. S.: Global increase in major tropical
847 cyclone exceedance probability over the past four decades, *Proceedings of the National*
848 *Academy of Sciences*, 117, 11975–11980, 2020.
- 849 Kunze, S.: Unraveling the Effects of Tropical Cyclones on Economic Sectors Worldwide:
850 Direct and Indirect Impacts, *Environmental and Resource Economics*,
851 <https://doi.org/10.1007/s10640-021-00541-5>, 2021.
- 852 Lai, Y., Li, J., Gu, X., Chen, Y. D., Kong, D., Gan, T. Y., Liu, M., Li, Q., and Wu, G.: Greater
853 flood risks in response to slowdown of tropical cyclones over the coast of China,
854 *Proceedings of the National Academy of Sciences*, 117, 14751–14755,
855 <https://doi.org/10.1073/pnas.1918987117>, 2020.
- 856 Laloyaux, P., de Boisseson, E., Balmaseda, M., Bidlot, J.-R., Broennimann, S., Buizza, R.,
857 Dalhgren, P., Dee, D., Haimberger, L., Hersbach, H., Kosaka, Y., Martin, M., Poli, P.,
858 Rayner, N., Rustemeier, E., and Schepers, D.: CERA-20C: A Coupled Reanalysis of the
859 Twentieth Century, *Journal of Advances in Modeling Earth Systems*, 10, 1172–1195,
860 <https://doi.org/10.1029/2018MS001273>, 2018.
- 861 Landsea, C.: Counting Atlantic tropical cyclones back to 1900, *Eos, Transactions American*
862 *Geophysical Union*, 88, 197–202, <https://doi.org/10.1029/2007EO180001>, 2007.
- 863 Landsea, C. W., Harper, B. A., Hoarau, K., and Knaff, J. A.: Can We Detect Trends in Extreme
864 Tropical Cyclones? *Science*, 313, 452–454, <https://doi.org/10.1126/science.1128448>,
865 2006.
- 866 Landsea, C. W., Glenn, D. A., Bredemeyer, W., Chenoweth, M., Ellis, R., Gamache, J.,



- 867 Hufstetler, L., Mock, C., Perez, R., Prieto, R., Sánchez-Sesma, J., Thomas, D., and
868 Woolcock, L.: A Reanalysis of the 1911–20 Atlantic Hurricane Database, *Journal of*
869 *Climate*, 21, 2138–2168, <https://doi.org/10.1175/2007JCLI1119.1>, 2008.
- 870 Landsea, C. W., Vecchi, G. A., Bengtsson, L., and Knutson, T. R.: Impact of Duration
871 Thresholds on Atlantic Tropical Cyclone Counts, *Journal of Climate*, 23, 2508–2519,
872 <https://doi.org/10.1175/2009JCLI3034.1>, 2010.
- 873 Lanzante, J. R.: Uncertainties in tropical-cyclone translation speed, *Nature*, 570, E6–E15,
874 <https://doi.org/10.1038/s41586-019-1223-2>, 2019.
- 875 Lee, R., Chen, L., and Ren, G.: A comparison of East-Asia landfall tropical cyclone in recent
876 reanalysis datasets--before and after satellite era, *Frontiers in Earth Science*, 10, 2023.
- 877 Lee, T.-C., Knutson, T. R., Nakaegawa, T., Ying, M., and Cha, E. J.: Third assessment on
878 impacts of climate change on tropical cyclones in the Typhoon Committee Region – Part
879 I: Observed changes, detection and attribution, *Tropical Cyclone Research and Review*,
880 9, 1–22, <https://doi.org/10.1016/j.tcr.2020.03.001>, 2020.
- 881 Lenzen, M., Malik, A., Kenway, S., Daniels, P., Lam, K. L., and Geschke, A.: Economic
882 damage and spillovers from a tropical cyclone, *Natural Hazards and Earth System*
883 *Sciences*, 19, 137–151, <https://doi.org/10.5194/nhess-19-137-2019>, 2019.
- 884 Leung, J. C.H., Qian, W., Zhang, P., and Zhang, B.: Geopotential-based Multivariate MJO
885 Index: extending RMM-like indices to pre-satellite era, *Clim Dyn*, 59, 609–631,
886 <https://doi.org/10.1007/s00382-022-06142-2>, 2022.
- 887 Li, J., Tian, Q., Shen, Z., Xu, Y., Yan, Z., Li, M., Zhu, C., Xue, J., Lin, Z., Yang, Y., and Zeng,
888 L.: Fidelity of global tropical cyclone activity in a new reanalysis dataset (CRA40),
889 *Meteorological Applications*, 31, e70009, <https://doi.org/10.1002/met.70009>, 2024.
- 890 Li, Y., Tang, Y., Li, X., Song, X., and Wang, Q.: Recent increase in the potential threat of
891 western North Pacific tropical cyclones, *npj Clim Atmos Sci*, 6, 1–8,
892 <https://doi.org/10.1038/s41612-023-00379-2>, 2023.
- 893 Malakar, P., Kesarkar, A. p., Bhate, J. n., Singh, V., and Deshamukhya, A.: Comparison of
894 Reanalysis Data Sets to Comprehend the Evolution of Tropical Cyclones Over North
895 Indian Ocean, *Earth and Space Science*, 7, e2019EA000978,
896 <https://doi.org/10.1029/2019EA000978>, 2020.
- 897 Mann, M. E., Sabbatelli, T. A., and Neu, U.: Evidence for a modest undercount bias in early
898 historical Atlantic tropical cyclone counts, *Geophysical Research Letters*, 34,
899 <https://doi.org/10.1029/2007GL031781>, 2007.
- 900 Mitchell, C. L.: The West Indian hurricane of September 10–20, 1928, *Monthly Weather*
901 *Review*, 56, 347–350, 1928.



- 902 Moon, I.-J., Kim, S.-H., and Chan, J. C. L.: Climate change and tropical cyclone trend, *Nature*,
903 570, E3–E5, <https://doi.org/10.1038/s41586-019-1222-3>, 2019.
- 904 Moon, M., Ha, K.-J., Kim, D., Ho, C.-H., Park, D.-S. R., Chu, J.-E., Lee, S.-S., and Chan, J.
905 C. L.: Rainfall strength and area from landfalling tropical cyclones over the North Indian
906 and western North Pacific oceans under increased CO₂ conditions, *Weather and Climate
907 Extremes*, 41, 100581, <https://doi.org/10.1016/j.wace.2023.100581>, 2023.
- 908 Moore, G. W. K. and Babij, M.: Iceland’s Great Frost Winter of 1917/1918 and its
909 representation in reanalyses of the twentieth century, *Quarterly Journal of the Royal
910 Meteorological Society*, 143, 508–520, <https://doi.org/10.1002/qj.2939>, 2017.
- 911 Murakami, H.: Tropical cyclones in reanalysis data sets, *Geophysical Research Letters*, 41,
912 2133–2141, <https://doi.org/10.1002/2014GL059519>, 2014.
- 913 Murakami, H. and Wang, B.: Patterns and frequency of projected future tropical cyclone
914 genesis are governed by dynamic effects, *Commun Earth Environ*, 3, 1–10,
915 <https://doi.org/10.1038/s43247-022-00410-z>, 2022.
- 916 Noy, I.: The socio-economics of cyclones, *Nature Clim Change*, 6, 343–345,
917 <https://doi.org/10.1038/nclimate2975>, 2016.
- 918 Parker, W. S.: Reanalyses and Observations: What’s the Difference? *Bulletin of the American
919 Meteorological Society*, 97, 1565–1572, <https://doi.org/10.1175/BAMS-D-14-00226.1>,
920 2016.
- 921 Pimm, S. L., Davis, G. E., Loope, L., Roman, C. T., Smith, T. J., and Tilmant, J. T.: Hurricane
922 Andrew, *BioScience*, 44, 224–229, <https://doi.org/10.2307/1312226>, 1994.
- 923 Qin, L., Zhu, L., Liu, B., Li, Z., Tian, Y., Mitchell, G., Shen, S., Xu, W., and Chen, J.: Global
924 expansion of tropical cyclone precipitation footprint, *Nat Commun*, 15, 4824,
925 <https://doi.org/10.1038/s41467-024-49115-1>, 2024.
- 926 Raavi, P. H. and Walsh, K. J. E.: Basinwise Statistical Analysis of Factors Limiting Tropical
927 Storm Formation from an Initial Tropical Circulation, *Journal of Geophysical Research:
928 Atmospheres*, 125, e2019JD032006, <https://doi.org/10.1029/2019JD032006>, 2020a.
- 929 Raavi, P. H. and Walsh, K. j. e.: Sensitivity of Tropical Cyclone Formation to Resolution-
930 Dependent and Independent Tracking Schemes in High-Resolution Climate Model
931 Simulations, *Earth and Space Science*, 7, e2019EA000906,
932 <https://doi.org/10.1029/2019EA000906>, 2020b.
- 933 Roberts, M. J., Camp, J., Seddon, J., Vidale, P. L., Hodges, K., Vannière, B., Mecking, J.,
934 Haarsma, R., Bellucci, A., Scoccimarro, E., Caron, L.-P., Chauvin, F., Terray, L., Valcke,
935 S., Moine, M.-P., Putrasahan, D., Roberts, C. D., Senan, R., Zarzycki, C., Ullrich, P.,
936 Yamada, Y., Mizuta, R., Kodama, C., Fu, D., Zhang, Q., Danabasoglu, G., Rosenbloom,



- 937 N., Wang, H., and Wu, L.: Projected Future Changes in Tropical Cyclones Using the
938 CMIP6 HighResMIP Multimodel Ensemble, <https://doi.org/10.1029/2020GL088662>, n.d.
- 939 Schreck, C. J., Knapp, K. R., and Kossin, J. P.: The Impact of Best Track Discrepancies on
940 Global Tropical Cyclone Climatologies using IBTrACS, *Monthly Weather Review*, 142,
941 3881–3899, <https://doi.org/10.1175/MWR-D-14-00021.1>, 2014.
- 942 Sharmila, S. and Walsh, K. J. E.: Recent poleward shift of tropical cyclone formation linked
943 to Hadley cell expansion, *Nature Clim Change*, 8, 730–736,
944 <https://doi.org/10.1038/s41558-018-0227-5>, 2018.
- 945 Slivinski, L. C.: Historical Reanalysis: What, How, and Why? *Journal of Advances in*
946 *Modeling Earth Systems*, 10, 1736–1739, <https://doi.org/10.1029/2018MS001434>, 2018.
- 947 Slivinski, L. C., Compo, G. P., Whitaker, J. S., Sardeshmukh, P. D., Giese, B. S., McColl, C.,
948 Allan, R., Yin, X., Vose, R., Titchner, H., Kennedy, J., Spencer, L. J., Ashcroft, L.,
949 Brönnimann, S., Brunet, M., Camuffo, D., Cornes, R., Cram, T. A., Crouthamel, R.,
950 Domínguez-Castro, F., Freeman, J. E., Gergis, J., Hawkins, E., Jones, P. D., Jourdain, S.,
951 Kaplan, A., Kubota, H., Blancq, F. L., Lee, T.-C., Lorrey, A., Luterbacher, J., Maugeri,
952 M., Mock, C. J., Moore, G. W. K., Przybylak, R., Pudmenzky, C., Reason, C., Slonosky,
953 V. C., Smith, C. A., Tinz, B., Trewin, B., Valente, M. A., Wang, X. L., Wilkinson, C.,
954 Wood, K., and Wyszynski, P.: Towards a more reliable historical reanalysis:
955 Improvements for version 3 of the Twentieth Century Reanalysis system, *Quarterly*
956 *Journal of the Royal Meteorological Society*, 145, 2876–2908,
957 <https://doi.org/10.1002/qj.3598>, 2019.
- 958 Slivinski, L. C., Compo, G. P., Sardeshmukh, P. D., Whitaker, J. S., McColl, C., Allan, R. J.,
959 Brohan, P., Yin, X., Smith, C. A., Spencer, L. J., Vose, R. S., Rohrer, M., Conroy, R. P.,
960 Schuster, D. C., Kennedy, J. J., Ashcroft, L., Brönnimann, S., Brunet, M., Camuffo, D.,
961 Cornes, R., Cram, T. A., Domínguez-Castro, F., Freeman, J. E., Gergis, J., Hawkins, E.,
962 Jones, P. D., Kubota, H., Lee, T. C., Lorrey, A. M., Luterbacher, J., Mock, C. J., Przybylak,
963 R. K., Pudmenzky, C., Slonosky, V. C., Tinz, B., Trewin, B., Wang, X. L., Wilkinson, C.,
964 Wood, K., and Wyszynski, P.: An Evaluation of the Performance of the Twentieth Century
965 Reanalysis Version 3, *Journal of Climate*, 34, 1417–1438, [https://doi.org/10.1175/JCLI-](https://doi.org/10.1175/JCLI-D-20-0505.1)
966 [D-20-0505.1](https://doi.org/10.1175/JCLI-D-20-0505.1), 2021.
- 967 Torn, R. D. and Snyder, C.: Uncertainty of Tropical Cyclone Best-Track Information, *Weather*
968 *and Forecasting*, 27, 715–729, <https://doi.org/10.1175/WAF-D-11-00085.1>, 2012.
- 969 Tory, K. J., Dare, R. A., Davidson, N. E., McBride, J. L., and Chand, S. S.: The importance of
970 low-deformation vorticity in tropical cyclone formation, *Atmospheric Chemistry and*
971 *Physics*, 13, 2115–2132, <https://doi.org/10.5194/acp-13-2115-2013>, 2013.



- 972 Truchelut, R. E. and Hart, R. E.: Quantifying the possible existence of undocumented Atlantic
973 warm-core cyclones in NOAA/CIRES 20th Century Reanalysis data, *Geophysical*
974 *Research Letters*, 38, <https://doi.org/10.1029/2011GL046756>, 2011.
- 975 Truchelut, R. E., Hart, R. E., and Luthman, B.: Global Identification of Previously Undetected
976 Pre-Satellite-Era Tropical Cyclone Candidates in NOAA/CIRES Twentieth-Century
977 Reanalysis Data, *Journal of Applied Meteorology and Climatology*, 52, 2243–2259,
978 <https://doi.org/10.1175/JAMC-D-12-0276.1>, 2013.
- 979 Tu, S., Xu, J., Chan, J. C. L., Huang, K., Xu, F., and Chiu, L. S.: Recent global decrease in the
980 inner-core rain rate of tropical cyclones, *Nat Commun*, 12, 1948,
981 <https://doi.org/10.1038/s41467-021-22304-y>, 2021.
- 982 Tu, S., Chan, J. C. L., Xu, J., Zhong, Q., Zhou, W., and Zhang, Y.: Increase in tropical cyclone
983 rain rate with translation speed, *Nat Commun*, 13, 7325, [https://doi.org/10.1038/s41467-](https://doi.org/10.1038/s41467-022-35113-8)
984 [022-35113-8](https://doi.org/10.1038/s41467-022-35113-8), 2022.
- 985 Ullrich, P. A., Zarzycki, C. M., McClenny, E. E., Pinheiro, M. C., Stansfield, A. M., and Reed,
986 K. A.: TempestExtremes v2.1: a community framework for feature detection, tracking,
987 and analysis in large datasets, *Geoscientific Model Development*, 14, 5023–5048,
988 <https://doi.org/10.5194/gmd-14-5023-2021>, 2021.
- 989 Wang, S. and Toumi, R.: More tropical cyclones are striking coasts with major intensities at
990 landfall, *Sci Rep*, 12, 5236, <https://doi.org/10.1038/s41598-022-09287-6>, 2022.
- 991 Wang, X. L., Feng, Y., and Swail, V.: North Atlantic wave height trends as reconstructed from
992 the 20th century reanalysis, *Geophysical Research Letters*, 39, 2012.
- 993 Yamaguchi, M., Chan, J. C. L., Moon, I.-J., Yoshida, K., and Mizuta, R.: Global warming
994 changes tropical cyclone translation speed, *Nat Commun*, 11, 47,
995 <https://doi.org/10.1038/s41467-019-13902-y>, 2020.
- 996 Ye, G., Leung, J.C.H., Dong, W., Xu, J., LI, W., Qian, W., Kong, H., and Zhang, B.: A
997 Reanalysis-Based Global Tropical Cyclone Tracks Dataset for the Twentieth Century
998 (RGTracks-20C) (v1.0.2). Zenodo. <https://doi.org/10.5281/zenodo.14411917>, 2024.
- 999 Yeasmin, A., Chand, S., and Sultanova, N.: Reconstruction of tropical cyclone and depression
1000 proxies for the South Pacific since the 1850s, *Weather and Climate Extremes*, 39, 100543,
1001 <https://doi.org/10.1016/j.wace.2022.100543>, 2023.
- 1002 Ying, M., Zhang, W., Yu, H., Lu, X., Feng, J., Fan, Y., Zhu, Y., and Chen, D.: An Overview of
1003 the China Meteorological Administration Tropical Cyclone Database, *Journal of*
1004 *Atmospheric and Oceanic Technology*, 31, 287–301, [https://doi.org/10.1175/JTECH-D-](https://doi.org/10.1175/JTECH-D-12-00119.1)
1005 [12-00119.1](https://doi.org/10.1175/JTECH-D-12-00119.1), 2014.
- 1006 Yoshida, K., Sugi, M., Mizuta, R., Murakami, H., and Ishii, M.: Future Changes in Tropical



- 1007 Cyclone Activity in High-Resolution Large-Ensemble Simulations, *Geophysical*
1008 *Research Letters*, 44, 9910–9917, <https://doi.org/10.1002/2017GL075058>, 2017.
- 1009 Zarzycki, C. M. and Ullrich, P. A.: Assessing sensitivities in algorithmic detection of tropical
1010 cyclones in climate data, *Geophysical Research Letters*, 44, 1141–1149,
1011 <https://doi.org/10.1002/2016GL071606>, 2017.
- 1012 Zhang, B., Zhang, R., Pinker, R. T., Feng, Y., Nie, C., and Guan, Y.: Changes of tropical
1013 cyclone activity in a warming world are sensitive to sea surface temperature environment,
1014 *Environ. Res. Lett.*, 14, 124052, <https://doi.org/10.1088/1748-9326/ab5ada>, 2019.
- 1015 Zhang, G.: Warming-induced contraction of tropical convection delays and reduces tropical
1016 cyclone formation, *Nat Commun*, 14, 6274, [https://doi.org/10.1038/s41467-023-41911-](https://doi.org/10.1038/s41467-023-41911-5)
1017 5, 2023.
- 1018 Zhang, X., Duan, Y., Wang, Y., Wei, N., and Hu, H.: A high-resolution simulation of
1019 Supertyphoon Rammasun (2014)—Part I: Model verification and surface energetics
1020 analysis, *Adv. Atmos. Sci.*, 34, 757–770, <https://doi.org/10.1007/s00376-017-6255-7>,
1021 2017.
- 1022 Zhao, M. and Held, I. M.: An Analysis of the Effect of Global Warming on the Intensity of
1023 Atlantic Hurricanes Using a GCM with Statistical Refinement, *Journal of Climate*, 23,
1024 6382–6393, <https://doi.org/10.1175/2010JCLI3837.1>, 2010.
- 1025 Zhu, L. and Quiring, S. M.: Exposure to precipitation from tropical cyclones has increased
1026 over the continental United States from 1948 to 2019, *Commun Earth Environ*, 3, 1–8,
1027 <https://doi.org/10.1038/s43247-022-00639-8>, 2022.
- 1028